THE FLORIDA STATE UNIVERSITY

COLLEGE OF ARTS AND SCIENCES

THE INTERANNUAL VARIABILITY OF THE UPPER OCEAN EQUATORIAL PACIFIC CURRENT SYSTEM

by

Louis Nash

A Thesis submitted to the
Department of Oceanography
in partial fulfillment of the
requirements for the degree of
Master of Science

APPROVED:

James J. O'Brien
Professor Directing Thesis

George Weatherly

Seymour L. Hess

[illegible]

W. J. Sturges 2 x Sept

W. J. Sturges 2 x Sept
Chairman, Department of Oceanography

December, 1981

ABSTRACT

The interannual variability of the Equatorial Pacific currents is investigated using data from a linear, one layer, reduced gravity model developed by Busalacchi and O'Brien (1981). Validity of the model is checked using observations. The model is forced by the Wyrtki and Meyers (1975a, b) wind data as subjectively analyzed by Goldenberg and O'Brien (1981) for 1961 through 1970. For the area 18°N to 12°S and 145°W to 155°W, and the years 1962 through 1970, the currents are dominated by the interannual variability. The North Equatorial Current is characterized by fast westerly flow alternating with slow easterly or westerly flow. The North Equatorial Countercurrent is found to be a narrow, often intense current that may appear or disappear in a time scale of two months or less. The South Equatorial current is fairly continuous, but highly variable in nature. The variability of the model's equatorial flow is found to be that of the Equatorial Undercurrent; the mean flow does not develop due to the lack of vertical resolution. Although feasable, no attempt is made to investigate the meandering of the undercurrent.

ACKNOWLEDGEMENTS

This work was made possible by the Division of Atmospheric Sciences, Climate Dynamics Section, National Science Foundation, under Grant ATM7920485, and the Office of Naval Research. The computer work was done on the CDC Cyber 74 and 730 at Florida State University.

I am deeply indebted to Dr. Jim O'Brien for his suggestion of a thesis topic and expert guidance. I would like to thank Drs. Seymour Hess, Richard Iverson, and Georges Weatherly for their comments, suggestions, and service on my thesis committee. Of course, this would have been impossible without the previous work of Mr. Antonio Busalacchi. I give him my heartiest thanks for his suggestions and help.

I would like to thank the members and staff of the Mesoscale Air-Sea Interaction Group for their support and friendship. In particular, I would like to acknowledge and thank Messrs. Jim Merritt and David Legler for their help with the computer, and Mrs. Patricia Teaf for typing.

I owe much to my mother, Viola, for encouraging me to get an education, and the U.S. Coast Guard for providing the opportunity. I owe a special thanks to my wife, Sharon, for her love, and understanding.

understanding.

TABLE OF CONTENTS

LIST OF TABLES

LIST OF FIGURES

7.	Same as Fig. 5, except for the NEC.	20
8.	Same as Fig. 6 except for the NECC.	21

1. INTRODUCTION

A linear numerical model of the tropical Pacific has been developed using as forcing the wind stress based on ship observations for the years 1961 to 1970 (Busalacchi and O'Brien, 1981). This is a description of the interannual variations in the position, strength and nature of the Pacific equatorial current system as revealed in model pycnocline and velocities. This study will primarily be concerned with the area 155°W to 145°W, 18°N to 12°S for the years 1962 to 1970. The interannual variations to be described are due to the first baroclinic mode.

For the purpose of this study, the Pacific equatorial current system consists of four currents and four complementary hydrographic features. The currents are the eastward flowing North Equatorial Countercurrent (NECC) and Equatorial Undercurrent and the westward flowing North Equatorial Current (NEC) and South Equatorial Current (SEC). The hydrographic features, from north to south, are the North Equatorial (NE) Ridge, Countercurrent (CC) Trough, Equatorial (EQ) Ridge, Equatorial (EQ) Trough, and South Equatorial (SE) Ridge. Unfortunately, as the model boundaries are at 12°S and 18°N near the ridges, the NE and SE Ridges are not defined in the model even though their slopes are.

The model and its limitations will be discussed further in the first section of Chapter 2. The governing equations and assumptions

The model and its limitations will be discussed further in the first section of Chapter 2. The governing equations and assumptions will be described with a brief discussion of the numerical techniques.

Some of the general features of the model will also be given. In the second section, there is a discussion of the history and features of the wind data. At the end of Chapter 2, there is a discussion of the observational knowledge of the area.

In Chapter 3, the seasonal signal and interannual variability of the individual currents are described and compared to observations. For continuity with past research, the seasonal signal is described for the zonally averaged section from 170°E to 140°W (Wyrtki, 1974a; Busalacchi and O'Brien, 1981). The variations with longitude are described by comparing different 10° zonally average sections and using current vector maps for 140°E to 140°W. The description of the interannual variability is for the section 155°W to 145°W. Some current and past observational studies concerned with this area are the Trade Wind Zone Oceanography (February 1964, - June 1965), the NORPAX Hawaii-Tahiti Test Shuttle Experiment from November 1977, to February 1978, and the Hawaii-Tahiti Shuttle Experiment from January 1979 to June 1980.

Instead of the usual lack of data, the main problem for this study was too much data, over 15 million pieces of data covering a tremendous area and spanning 10 years. The first year's data was excluded from much of the study due to noise from the initialization of the model. There may be some noise left in 1962, but is is probably small. Even then, the data base is huge, and many of the more common methods of data handling fail.

The data base record is too short for spectral analysis to show data handling fail.

The data base record is too short for spectral analysis to show the interannual variations. There are too many events, with a time

scale of a few months for current vectors maps to give an adequate description of the variations without using an unmanageable number of maps. The problem becomes more manageable by limiting the discussion to one meridional section and using the currents zonal nature. Zonally averaging over 10° reduces the small perturbations due to local winds, but leaves intact the major or large scale events. Averaging over a larger distance smooths or removes many of the interesting features. Hindsight suggests that averaging over a smaller distance, such as 5°, may have been better. Zonally averaging over 10° distorts the flow attributable to either planetary waves or eddies, enough that in some cases, they may appear to be a continuation of the current. This necessitates the use of other meridional sections and current vector maps as a check.

The philosophy behind this study is that whereas; observations are limited in scope and duration due to the constraints of finance and logistics; numerical models can provide very dense output, subject to different limitations. The validity of the model, which depends on the assumptions made, numerical procedures used and inputs, can be determined by comparisons with observations. Thus insight into observed phenomenon may be gained and/or new, as of yet unobserved phenomenon suggested. A valid model can pose questions, and provide a framework or parameters for further observational efforts, plus reinterpretation of past observations.

2. REVIEW OF MODEL AND OBSERVATIONS

a. THE MODEL

The data for this study were generated in a model by Busalacchi and O'Brien (1981). It is a linear, one layer, reduced gravity, transport model on a equatorial beta-plane (see Fig. 1). The model dissipation mechanism is in the form of a constant horizontal eddy viscosity and wind stress as a body force. The interface between layers is permitted to move, and the barotropic mode is suppressed. The ocean is assumed to be a Boussinesq fluid.

The model equations are

$$\frac{\partial \vec{V}}{\partial t} = -\beta y \hat{k} x \vec{V} - c^2 \nabla h + \frac{\vec{\tau}}{\rho} + A \nabla^2 \vec{V}$$

$$\frac{\partial h}{\partial t} = -\nabla \cdot \vec{V}$$

where $\vec{V} = U\hat{i} + V\hat{j}$

U and V are the zonal and meridional transports, and h is the deflection of the interface. The initial depth of the upper layer is 300 m, and β is 2.25×10^{-11} m^{-1} s^{-1}. A constant horizontal eddy viscosity, A, of 100 m^2 s^{-1} is used. See Appendix for list of symbols.

A staggered grid with a 40 km grid spacing and a two hour time step, which satisfies the C-F-L stability condition, is used. All first order derivatives are replaced by standard second-order center

order derivatives are replaced by standard second-order center

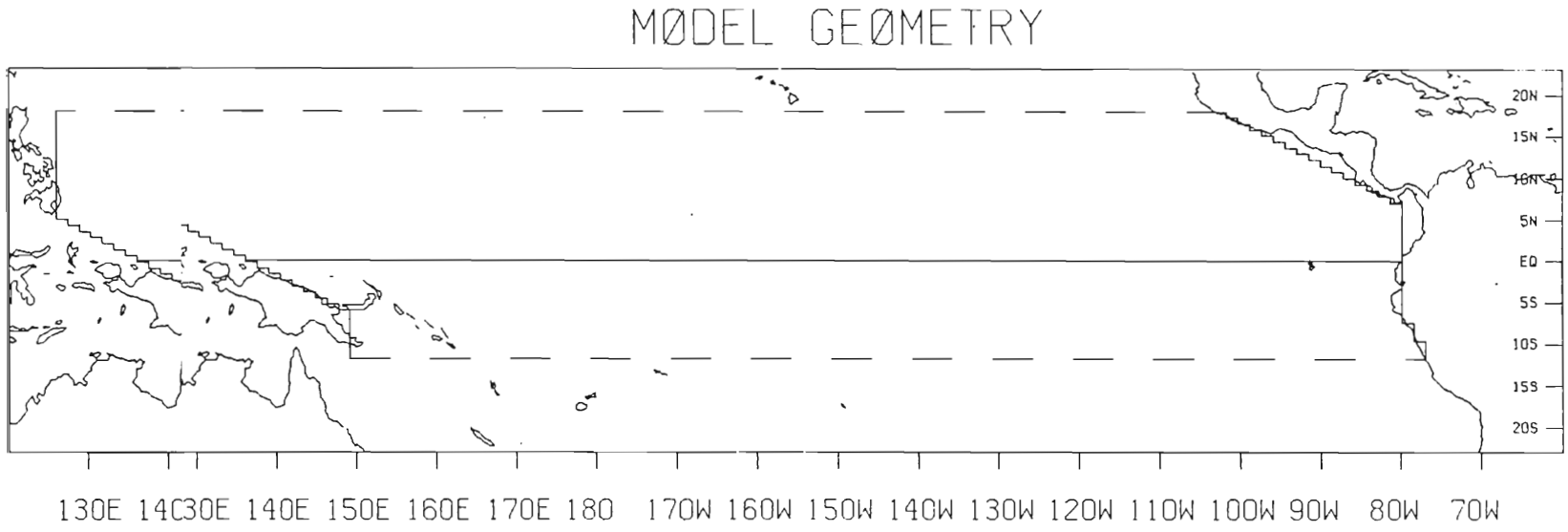

Figure 1. Comparison of model geometry with Pacific Ocean. The model extends from from 12°S to 18°N and 126°E to 77°W with no-slip east and west boundaries and open north north and south boundaries (dashed lines). (Fig. 1 of Busalacchi and O'Brien, 1980).

differences. The Coriolis terms are centered in time and averaged in space while the diffusive terms are treated by the Dufort-Frankel scheme. A leapfrog scheme is used for time derivatives. To prevent time splitting, a forward difference scheme is used every five days.

The model does not include bottom topography, any thermohaline circulation or other thermodynamics. The reduced gravity formulation retains only the gravest (first) baroclinic mode. The lack of vertical resolution does not allow the Equatorial Undercurrent to develop fully as a separate current. Ignoring friction, the model's physics at the equator is given by

$$\frac{\partial \vec{V}}{\partial t} = -C^2 \nabla h + \frac{\vec{\tau}}{\rho}$$

The wind stress of the trades could be expected to drive a westward surface jet, while the pressure gradient would drive an eastward current. If the transport of the surface jet is of a smaller magnitude than that of the Undercurrent, the interannual variability at the Equator can be taken as indicative of that of the Undercurrent. This is possible as the Undercurrent's position is not known to deviate far from the equator (Knauss, 1966, Taft and Jones, 1973).

There is a general uplifting of the model's interface during the run. This is caused by a net curl of the wind stress and the open boundary conditions. As the location of the northern and southern boundaries prevent the NE and SE ridges from being well defined, the lack of physics outside of the model may prevent the ridges from

lack of physics outside of the model may prevent the ridges from

reaching quasi-stability. The result would be smaller height differences between ridges and troughs. In fact, one of the major differences between the model and observations is that the height differences are 1/3 to 1/2 the observed, and therefore the currents are much less. However, it is well known that one baroclinic mode models tend to preserve phase changes but the amplitude of horizontal currents and vertical displacements are reduced. Another major difference is that all major features are shifted roughly 2° southward (Busalacchi and O'Brien, 1980).

With the previously mentioned exceptions, all of the major hydrographic features can be seen in the mean field of the upper layer thickness (Fig. 2). The CC Trough runs at an angle to the equator that coincides with the paths of Rossby waves as discussed by Busalacchi and O'Brien (1980). The trough has a sharper poleward slant east of 160°W. With a similar angle, the Equatorial Trough can be seen from 160°W to 5°S, 110°W. In the Northern Hemisphere's Fall, there is an eastward current on the northern slope of the Equatorial Trough, as reported in the literature, (Tsuchiya, 1974; Busalacchi and O'Brien, 1980).

b. WIND DATA

The model is driven by the mean monthly wind stress for the years 1961 to 1970 from Wyrtki and Meyers (1975a, b) as subjectively analyzed by Goldenberg and O'Brien (1981).

Wyrtki and Meyers (1975a, b,) created maps of the average monthly winds and wind stress over the Pacific Ocean for 2° x 10° latitude-longitude quadrangles from 5 million ship wind observations between

winds and wind stress over the Pacific Ocean for 2° x 10° latitude-longitude quadrangles from 5 million ship wind observations between

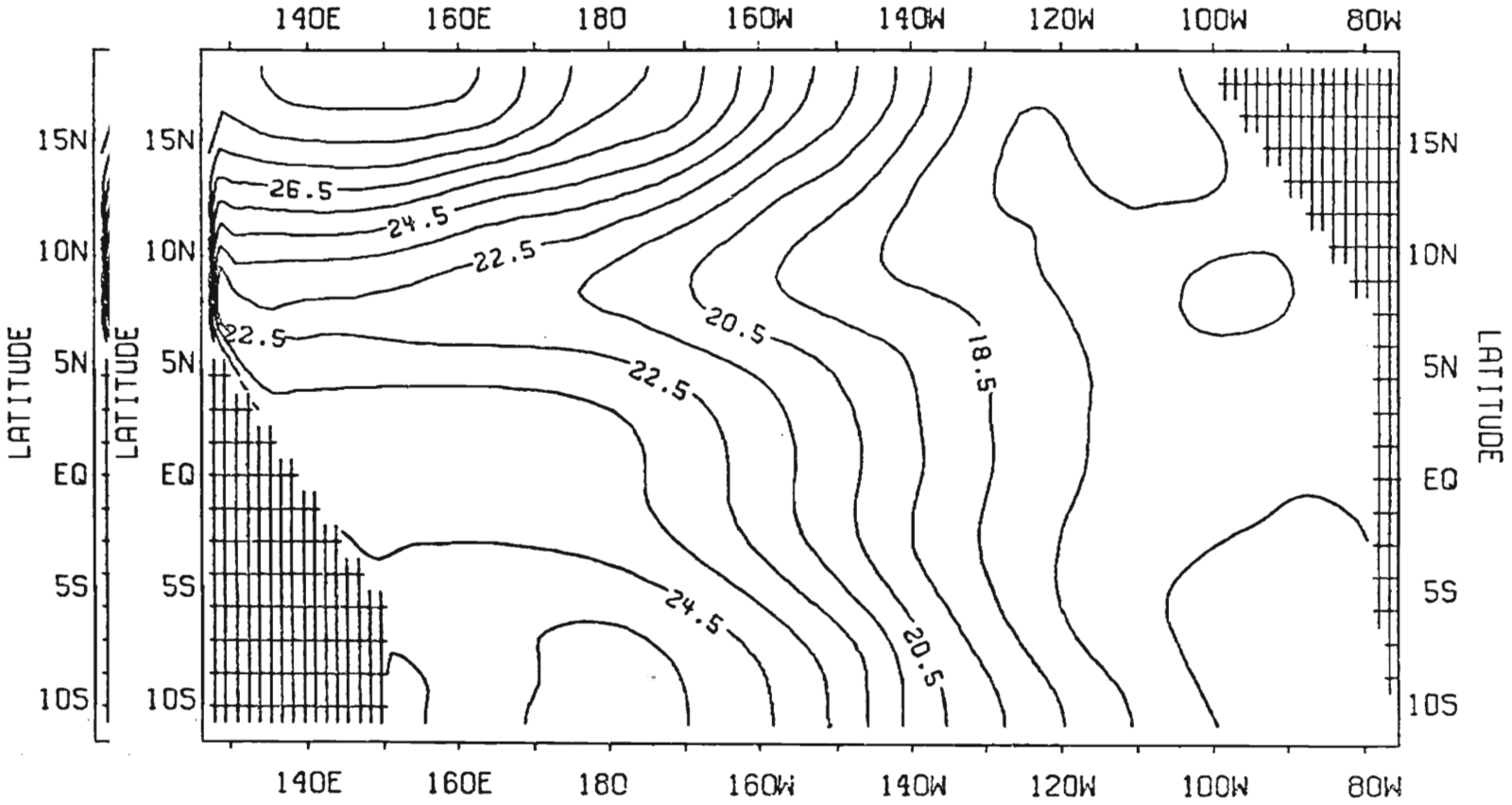

Fig. Fig. 2 The mean thickness of the model's upper layer for the period 1961-1970.-1970. Contour intervals and units are 10m. The hatched area denotes land. Note the c the classical pileup of water in the western basin, and the Countercurrent Trough extgh extending from 7°N, 130°E to 10°N, 130°W, and the Costa Rica Dome at 8°N, 98°W.

30°N to 30°S for the years 1900-1973, to study both the seasonal and interannual variability of the Pacific Ocean trade wind field. On this initial data processing, all observations greater than 40 m s^{-1} during typhoons were excluded.

To obtain a data set suitable for computer modelling, the Wyrtki and Meyers data was subjectively analyzed by Goldenberg and O'Brien (1981) for each month of 1961 thru 1970 onto a 2° square grid, to match the approximate land boundaries used in modelling. The methodology consisted of drawing separate scalar maps of the two components of wind stress using standard synoptic techniques such as climatology, continuity and topography (near boundaries). Climatology was used to fill the regions where little or no data existed. All monthly averages were weighted by the number of observations and checked for sign errors. Very large monthly average values that produced unrealistically strong gradients were adjusted or discarded and the maps were digitized onto a 2° square grid.

The wind spectrum is essentially white, with an area of high interannual variability center just north of the equator in the central Pacific, and a band of high annual variability lying approximately along the mean position of the ITCZ, extending east of the dateline (Goldenberg and O'Brien, 1981). The interannual variability in the winds is responsible for the occurence of El Niño events. The annual variability in the meridional stress (τ_y) is due to the seasonal variation of position of the ITCZ, while that of the magnitude (τ) and zonal stress (τ_x) is due to variation (seasonal oscillation) in the Northeast Trades (Goldenberg and O'Brien, 1981). In three longitudinal

bands, Goldenberg and O'Brien (1981) found that for 11°N, 124-144°E, the wind stress is dominated by the Southeast Asian Monsoon, and that the annual peak in energy in τ_x and τ_y combine to form both an annual peak and semiannual peak in τ. In the eastern Pacific, 11°N, 122-142°W, along the mean position of the ITCZ, they found a prominent annual and small semiannual signal for τ, τ_x and τ_y. They also found some power in τ, τ_x in some very low frequencies (less than 0.1 cycles/year) and some energy in τ_y around 3.3 years, though not at a significant level. In the central Pacific, at 3°S, 178°E-162°W, centered on Canton Island, the τ and τ_x spectrums are flat except for some energy around a period of about 2.2 to 2.5 years, while the τ_y spectrum has a significant annual peak (Goldenberg and O'Brien, 1981).

c. OBSERVATIONS

Even though there have been several major investigative efforts in the tropical Pacific, the observational coverage still leaves much to be desired. There are always trade-offs of area, duration, and density of coverage due to the constraints of logistics and finance. The longest running records are those of island sea levels for the central and western tropical Pacific (see Fig. 3). Wyrtki used the sea level records and geostrophy to monitor equatorial currents for 1950 to 1970 and starting again in 1974. Wyrtki (1974a,b) formed the zonally and time averaged dynamic height profile relative to 500 dbar for 140°W to 170°E and 30°N to 20°S using a collection of hydrographic stations. The monthly mean sea level anomaly as determined for each station from the 20 year mean, was linearly interpolated in the north-south

The monthly mean sea level anomaly as determined for each station from the 20 year mean, was linearly interpolated in the north-south

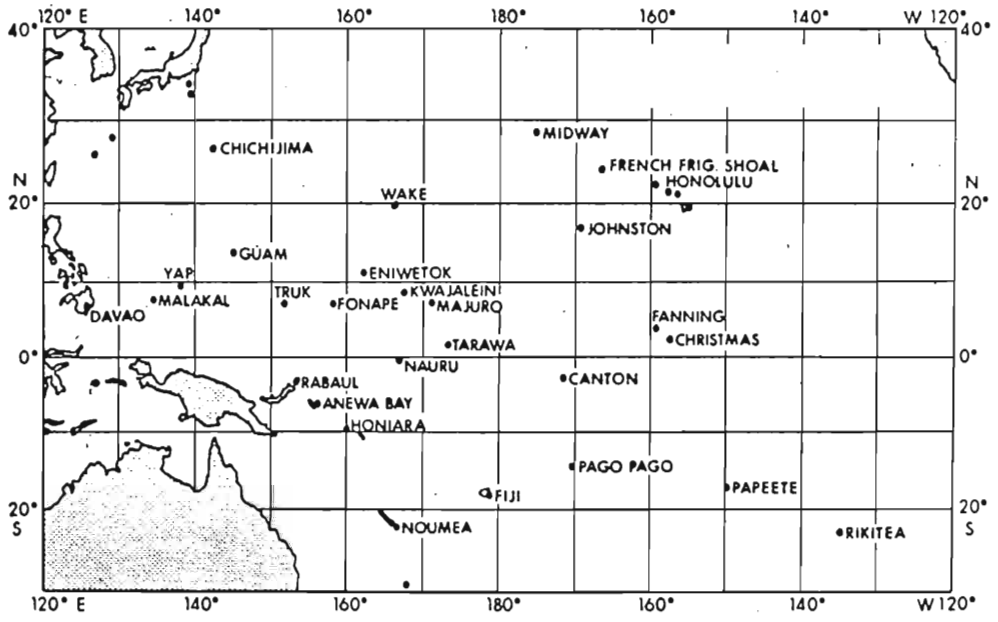

Figure 3. Chart showing many of the Pacific islands. The period and location of the sea level gages used by Wyrtiki (1974b) are: 1950-70, Midway, Honolulu, Johnston, Kwajalein, and Pago Pago; 1950-67, Canton; 1956-70, Christmas; 1957-64, Tahiti (Papeete) (Fig. 2 of Wyrtki, 1979).

direction between stations and superimposed on the average dynamic height profile. The sea level difference between successive ridges and troughs is taken as an indication of the corresponding current strength. The drawbacks of the method are: zonally averaging causes some meridional smoothing due to zonal differences; spacing between stations, both in latitude and longitude, does not permit determinations of smaller scale features. Also the sea level differences across currents do not account for change in slope due to variations in position of the topographic features.

In the western Pacific, cooperative study of the Kuroshio cruises have been conducted during the last two weeks of January from 1967 to 1974 for the area 127 to 137°E, 34°N to 1°S (Masuzawa and Nagasaka, 1975). From March 1967 to May 1968, the ORSTOM Centre of New Caledonia conducted the Cyclone cruises, which included transects from 20°S to 4°N along 170°E (Magnier, et al., 1973). In the central and eastern Pacific, there have been several studies. Specifically for the Equatorial Undercurrent, the Dolphin Expedition, in April thru June 1958, investigated the region from 140°W to 89°W, followed in September thru November 1961, by the Swan Song Expedition, which did meridional transects from 5°N to 5°S along 140°W, 118°W, 96°W and 87°W, plus stations around Galapagos islands (Knauss, 1960, 1966). From February 1964 to June 1965, the Trade Wind Zone Oceanography Investigation conducted 16 cruises in the area 26°N to 10°N, 148°W to 157°W (Seckel, 1968). An intensive study of the eastern Pacific, consisting of 7 two month cruises plus ships of opportunity, floats, etc., EASTROPAC study
1968). An intensive study of the eastern Pacific, consisting of 7 two month cruises plus ships of opportunity, floats, etc., EASTROPAC study

the area 20°N to 20°S, 126°W and east, from February 1967 to January 1968 (Love, 1972). The Piquero Expedition investigated the Equatorial Undercurrent from June to August 1969 for the region 115.5°W to 93.5°W (Taft and Jones, 1973). The NORPAX Hawaii-Tahiti Test Shuttle Experiment was conducted with nearly monthly observations in the area 20°N to 17.5°S, 150°W to 158°W from November 1977 to February 1978, and the shuttle from January 1979 to June 1980 (Wyrtki, et al., 1981).

3. VARIABILITY OF THE EQUATORIAL PACIFIC CURRENT SYSTEM

In this section, the seasonal signal and interannual variability of the individual currents, as they appear in the model, will be discussed and compared with observations. The seasonal signal is defined as the average year for the period 1961-1970. The differences in phase of the seasonal signal will be discussed using the current as given in Table 1 for zonally averaged sections 170°E to 140°W, 155°E to 165°E, and 155°W to 145°W. Except for the Equatorial Undercurrent, each current's variations with longitude will be discussed separately for 140°E to 140°W using current vector diagrams for the middle of March, June, September and December. All velocities for the discussion of the seasonal cycle are determined using actual upper layer thickness.

The interannual variability discussion will be based on the zonally averaged section centered on 150°W. Due to the long term upwelling of the thermocline, the velocities for the UYT (contour of zonal velocity in latitude and time) diagrams are determined using a constant upper layer thickness of 200 m. The meridionally and zonally averaged currents, as defined in Table 1, use the actual upper layer thickness.

a. SEASONAL CYCLE

Phase Relationship The seasonal cycle of the Pacific equatorial current system is well-known. Wyrtki (1974a) has shown that the system can be considered as consisting of two subsets, each containing a westward and eastward current. The Southern Hemisphere subset.
system can be considered as consisting of two subsets, each containing a westward and eastward current. The Southern Hemisphere subset,

TABLE 1. The east-west velocities of the model currents averaged from 1961 to 1970, over the respective latitudes for the given bands of longitudes. Eastward is positive.

Current	170°E to 140°W		155°W to 145°W		155°E to 165°E	
	Lat.	Mean Vel. (10^{-2} m s^{-1})	Lat.	Mean Vel. (10^{-2} m s^{-1})	Lat.	Mean Vel. (10^{-2} m s^{-1})
NEC	11°N 15°N	-6.1	12°N 15.5°N	-4.4	10°N 16°N	-6.4
NECC	4°N 7°N	9.0	4.5°N 7°N	8.2	4°N 7°N	8.0
EQC	2°S 2°N	3.3	2°S 2°N	4.3	2°S 2°N	3.9
SEC	3°S 7°S	-8.3	4.5°S 6°S	-9.3	3°S 4.5°S	-4.5

consisting of the SEC and Undercurrent, is the strongest in the Northern Hemisphere's spring and weakest in the fall. The Northern Hemisphere's subset, consisting of the NECC and NEC, varies almost 180° out of phase with the Southern Hemisphere (Wyrtki, 1974a; Busalacchi and O'Brien, 1980).

In the model for the section 170°E to 140°W, there seems to be a lag of 3 months between the strongest part of the SEC and Undercurrent (see Fig. 4). This lag may be due to the equatorial signal being a mixture of that of the SEC and Undercurrent. This would agree with the classical picture of the Undercurrent laying beneath the Equatorial Trough, with the SEC traveling along on both slopes. But the section for 155°E to 165°E show that the SEC and Undercurrent are in phase (see Figs. 5 and 6). In general, the sections at 155-145°W lead the sections at 155°E to 165°E (see Figs. 5, 6, 7 and 8). This difference is expected if the locally induced seasonal cycle is modified by westward propagating Rossby waves (Busalacchi and O'Brien, 1980).

North Equatorial Current In March (see Fig. 9), the NEC at 140°W is centered on 9°N. Between 160°W and 165°W, the current shifts sharply to 12°N and broadens. The highest velocities are found in the east and west. In June (see Fig. 10), the core of the NEC is centered on 10 to 11°N. It reaches its highest velocities between 160°W and 140°W where it is fed by the NECC. The NEC in turn feeds the NECC around 160°W to 165°W. In the west, the NEC is broad and consistent. In September (see Fig. 11), the NEC's core at 140°W lies around 14 to 15°N. The current shifts southward to 11 to 12°N by 175°E and broadens west of

(see Fig. 11), the NEC's core at 140°W lies around 14 to 15°N. The current shifts southward to 11 to 12°N by 175°E and broadens west of

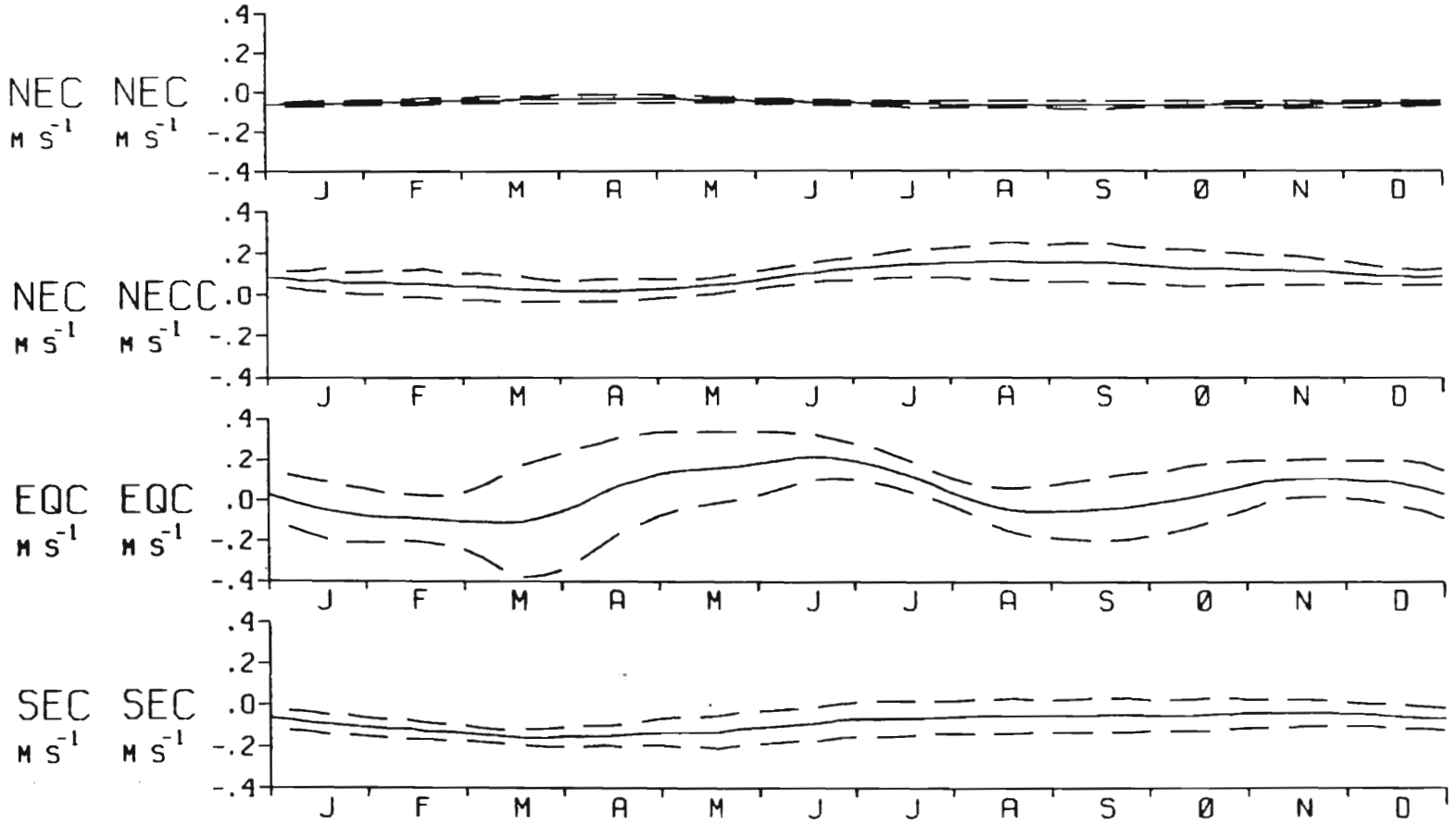

Figure 4. The east-west velocities of the currents, for the section 170°E to 140°W, as defined in TABLE 1, for the average year. Positive velocities are eastward. Dashed lines are one root mean square of the error from the average year, where the R.M.S.E. is defined as $(\frac{1}{N}\sum_{i=1}^{N}(x_i-\bar{x})^2)^{1/2}$; N ≡ number of observations, $\bar{x}$ ≡ mean.

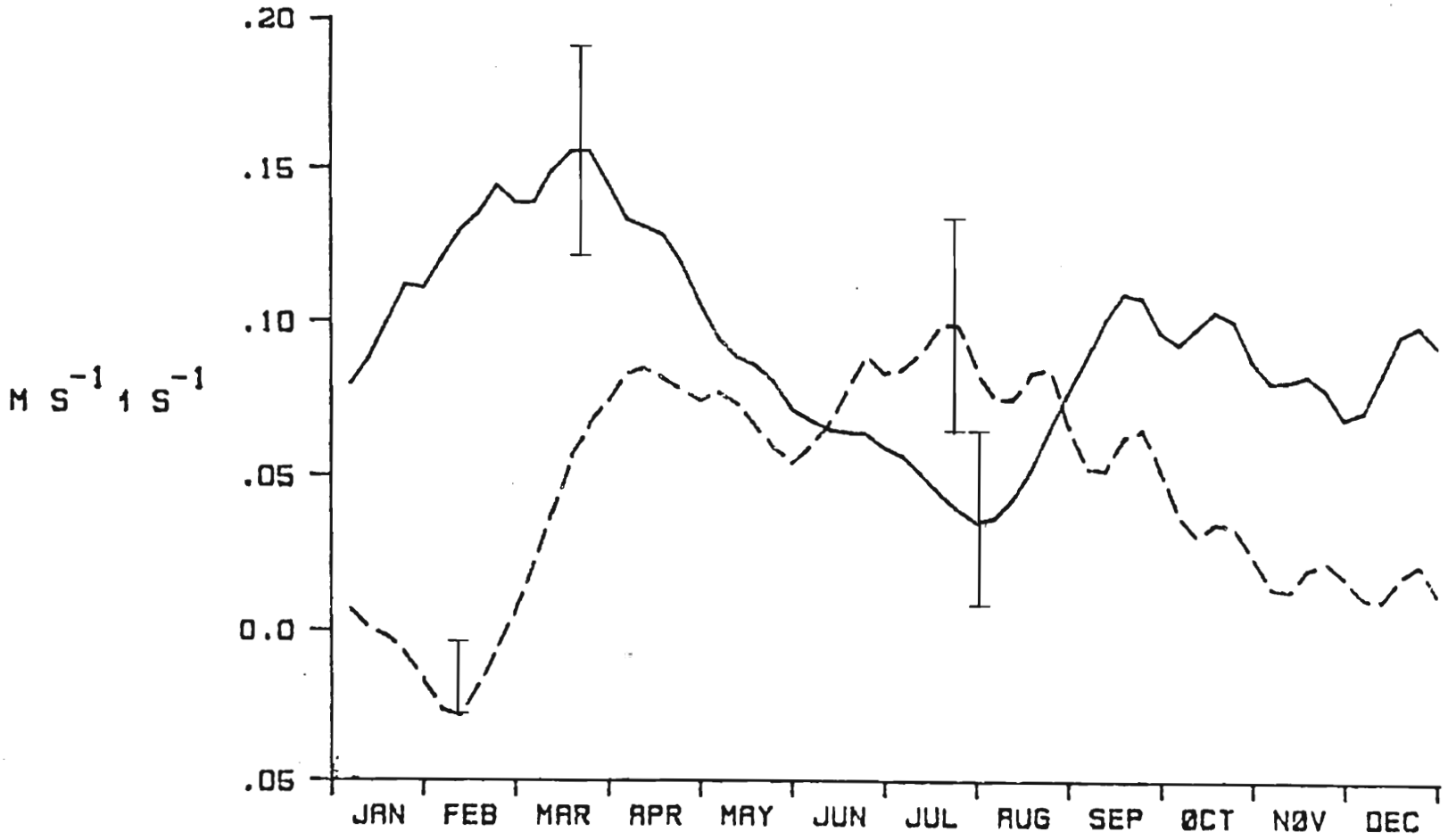

Figure 5. The zonal velocities for the average year for the SEC as defined in Table 1 for sections 155°E to 165°E (dashed line), and 155°W to 145°W, (solid line). Velocities are determined using actual upper layer thickness. Velocity at the figure's top is westward. Complete error bar is 2 standard error of the means. The standard error of the mean is defined as $\frac{R.M.S}{(N)^{1}}$ $\frac{R.M.S.E.}{(N)^{1\,2}}$; where symbols are as for Fig. 4.

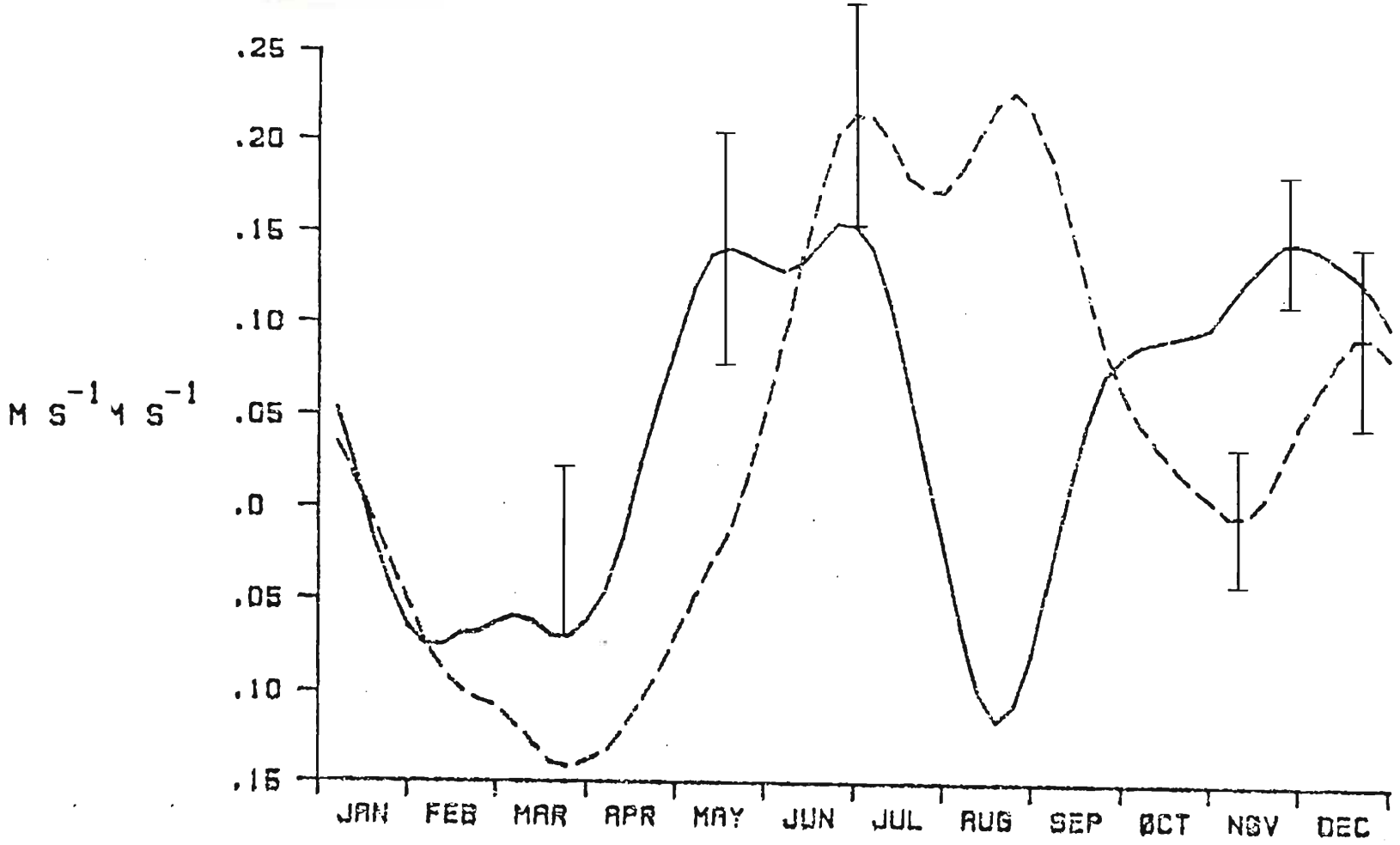

Figure 6. Same as Fig. 5 except for the Equatorial Undercurrent and velocity at the figur figure's top is eastward.

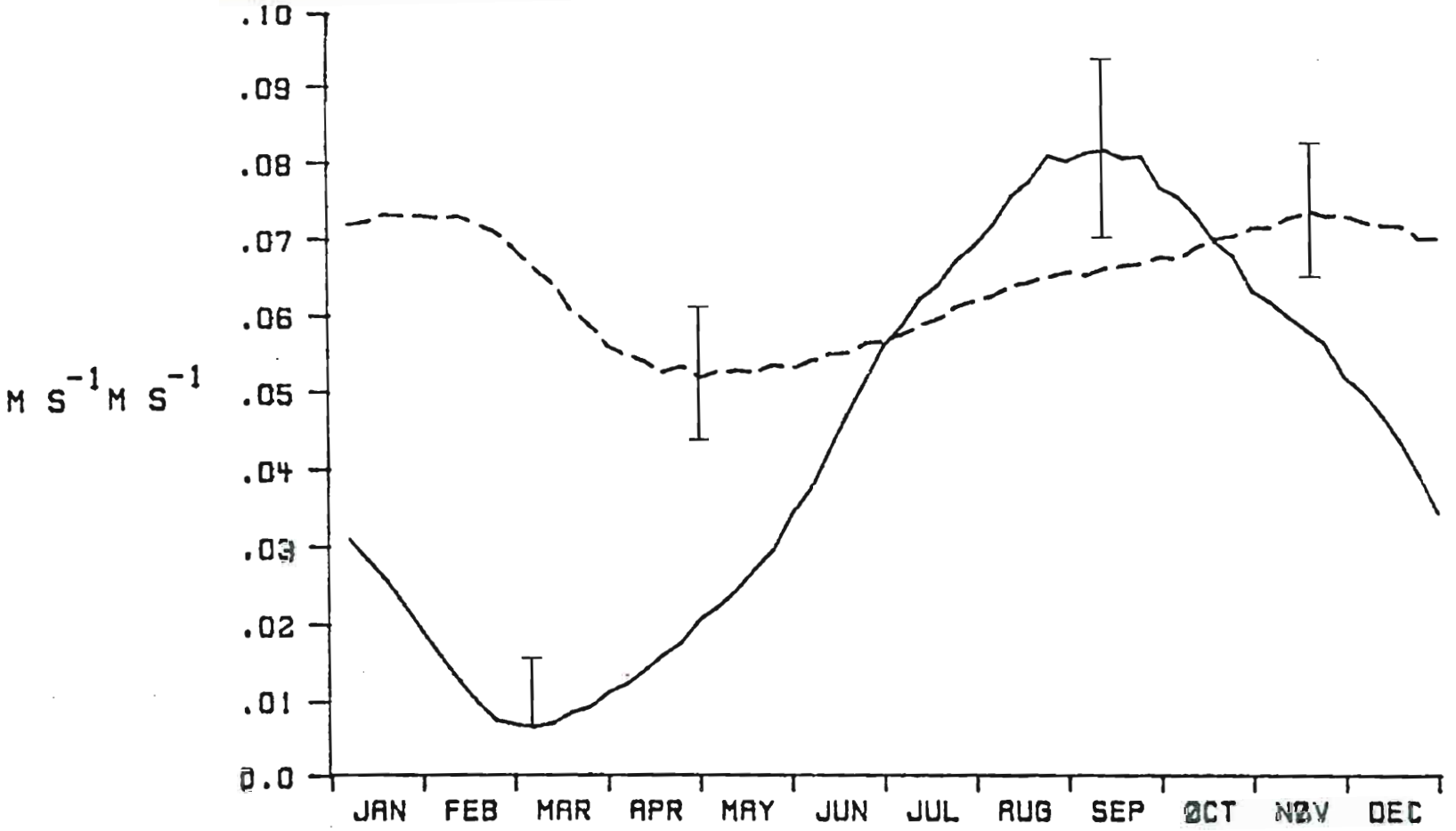

Figure 7. Same as Fig. 5, except for the NEC.

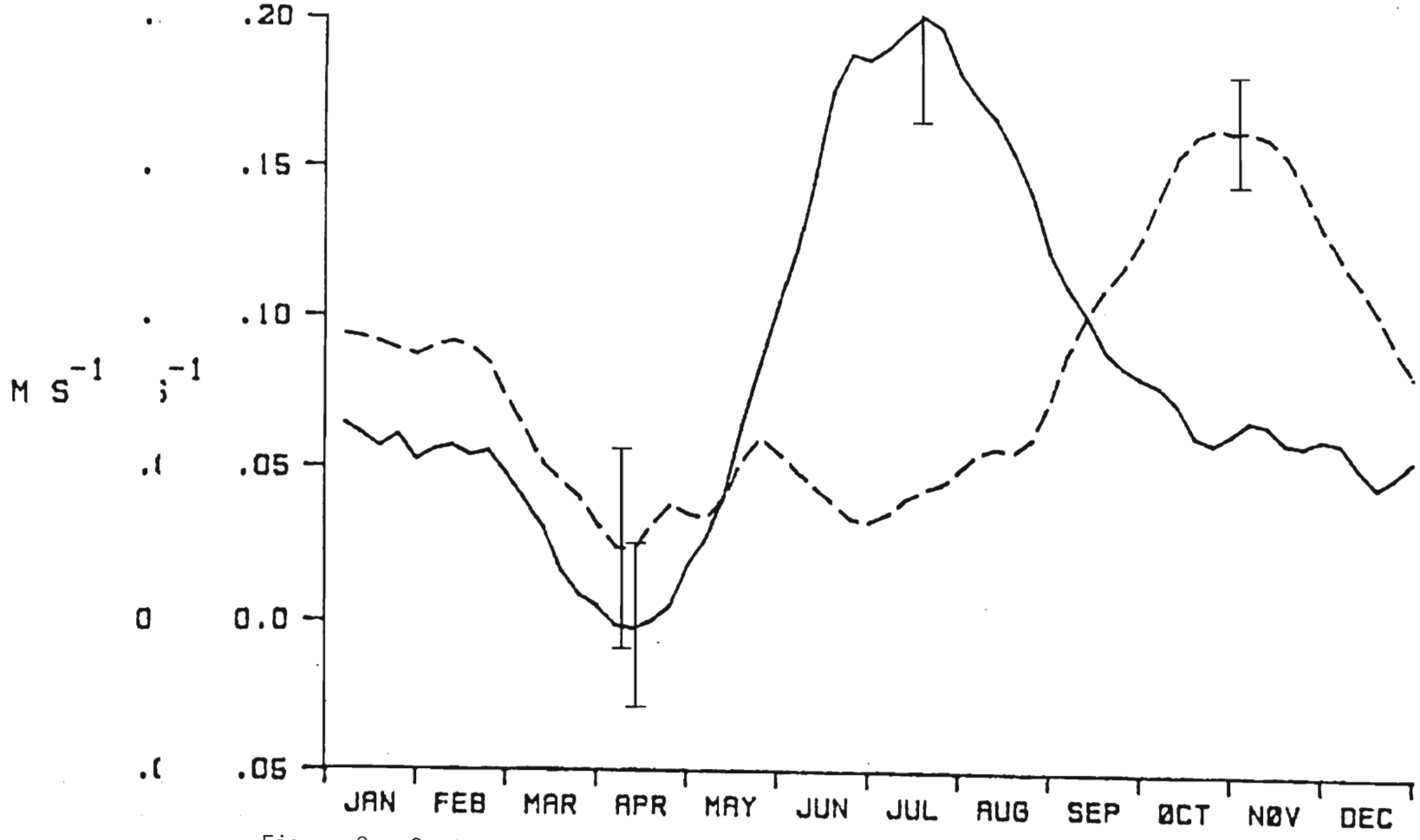

Figure 8. Same as Fig. 6 except for the NECC.

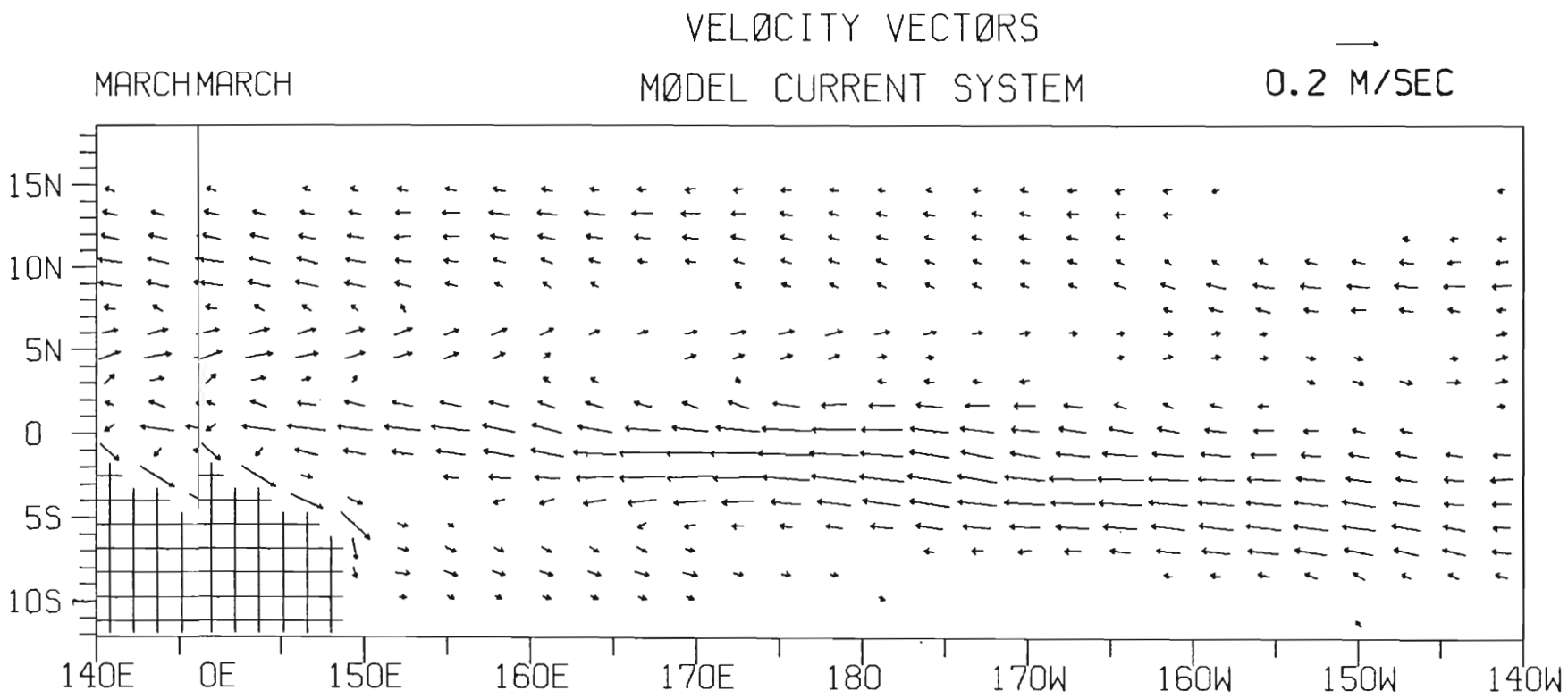

Figure 9igure 9. Current vectors for a section of the model for the middle of March. Velocities were determined usined using actual upper layer thickness. The figure is a 10 year average using the timestep corresponding ponding to the middle of March for each year. The hatched area is land. Vectors less than 0.03 m s^{-1} wei s^{-1} were not drawn.

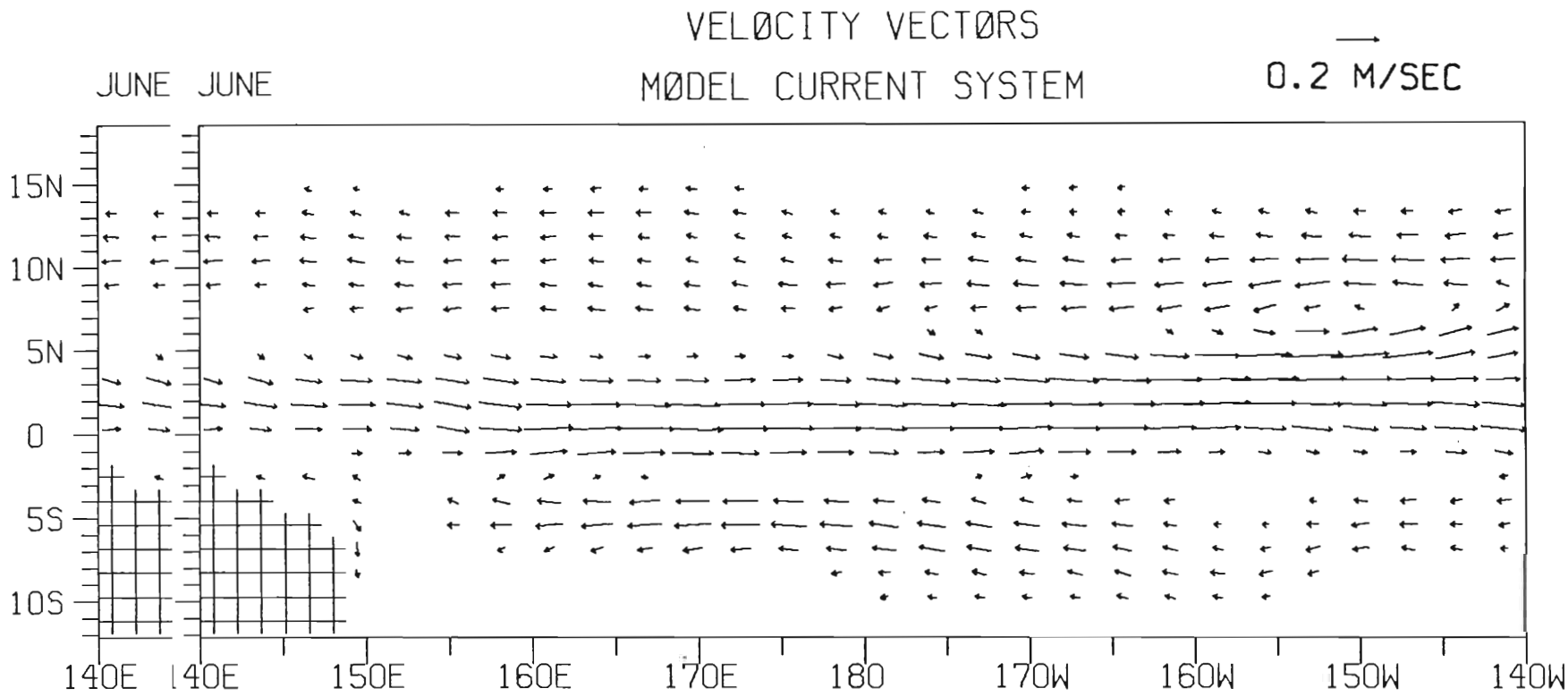

Figure Figure 10. Same as Fig. 9 except for June.

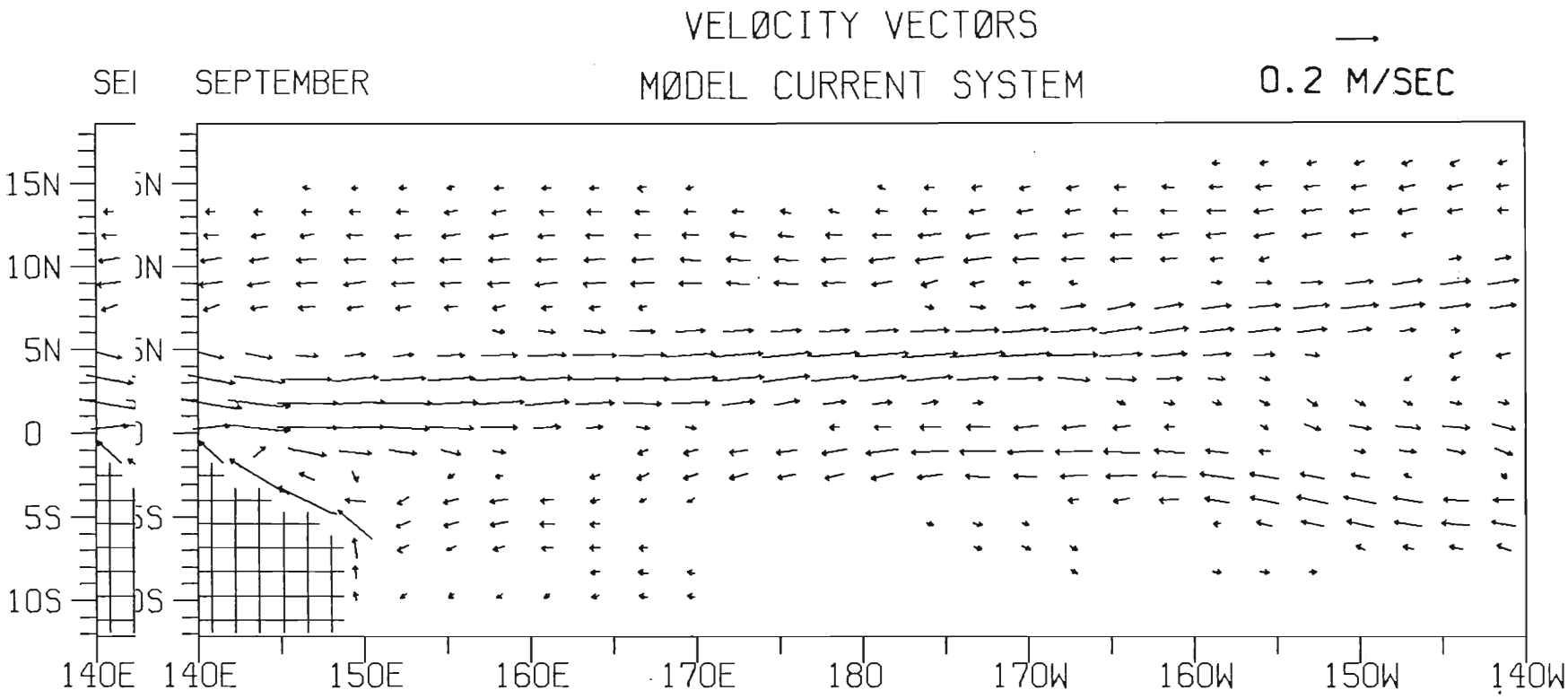

Figure Figure 11. Same as Fig. 9 except for September.

the dateline. The highest velocities are around 175°W. The weakness and narrowness of the current around 140°W may be due to the proximity of the boundary. In December, (see Fig. 12), the NEC is very weak and narrow. The core lies around 15°N at 140°W, and shifts southward as the current broadens to 11°N at 140°E. The NEC appears to be fed by the NECC from 140°W to 140°E. The highest velocities are found around the dateline.

North Equatorial Countercurrent In March (see Fig. 9), the NECC is weak and narrow with the core centered on 5 to 6°N for 140°E to 155°W. The current makes a rapid southward shift at 155°W to 3 to 4°N. The NECC is the strongest in the west where it is fed by the SEC and feeds the NEC. In June (see Fig. 10), the NECC is its strongest and the core lies on 1 to 3°N from 140°E to 140°W. The NECC is fed by both the SEC and NEC from 140°E to 150°E, and 175°W to 170°W. The SEC also feeds it between 155°E and 165°E, while the NEC feeds the NECC around 160°W and in turn is fed by the NECC between 145°W and 140°W. In September (see Fig. 11), the NECC is narrower except west of 165°E, but still strong. At 140°E, the core of the NECC is located at 2 to 3°N, shifting to 4 to 5°N by 170°W to 165°W. Around 155°W, the current splits into two parts. The major part shifts northward to 7 to 8°N. The southern part shifts to the Equator, and may be either the Undercurrent or the previously mentioned Tsuchiya Current (Tsuchiya, 1974; Busalacchi and O'Brien, 1980). In December (see Fig. 12), the NECC is weaker and generally shifted northward. The core of the NECC is located at 2 to 3°N from 140°E to 165°E. Between 170°E and the dateline, the core

generally shifted northward. The core of the NECC is located at 2 to 3°N from 140°E to 165°E. Between 170°E and the dateline, the core

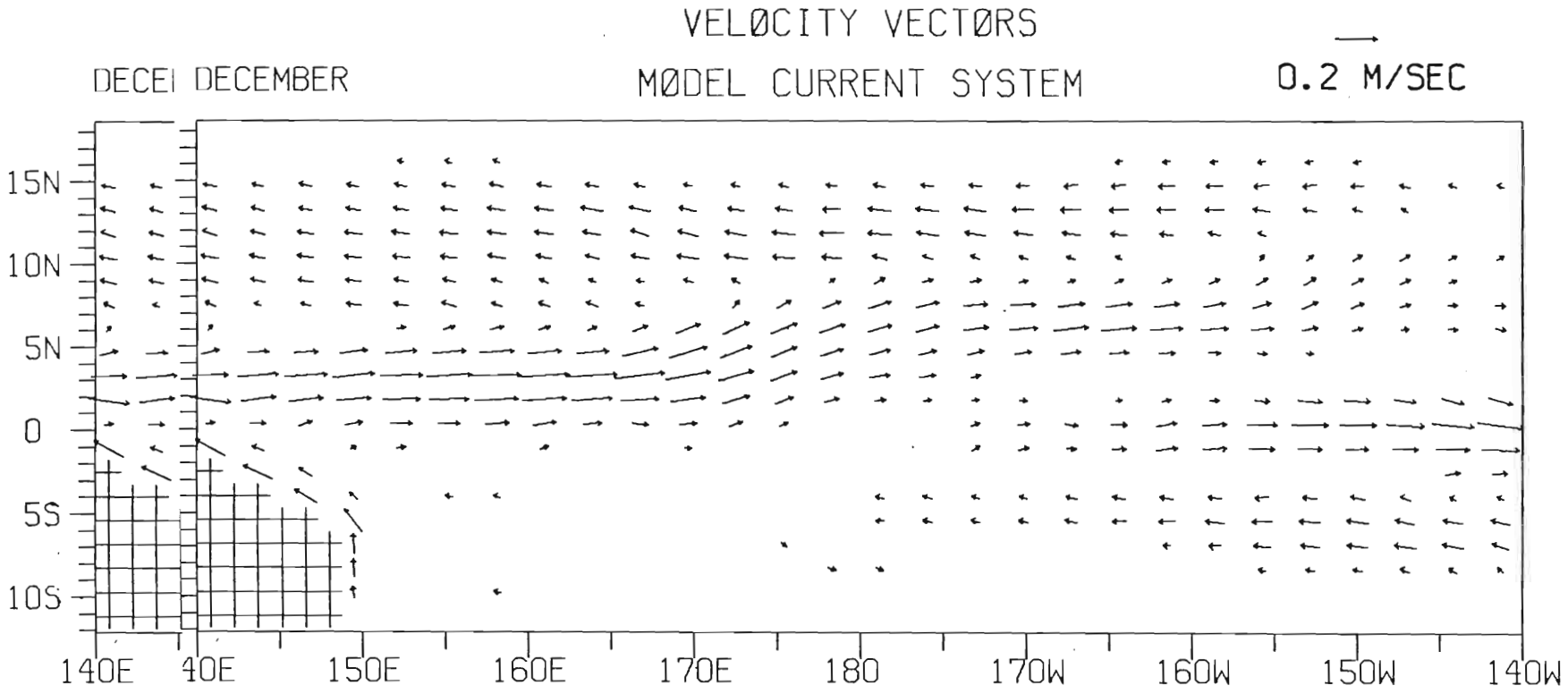

Figure Figure 12. Same as Fig. 9 except for December.

shifts northward to 5 to 6°N. Either the Tsuchiya Current or Equatorial Undercurrent is evident east of 175°W. The countercurrent shifts north to 6 to 7°N by 170°W. East of 160°W, it curves slightly northward and weakens. From 150°E to 140°W, the NECC appears to feed the NEC.

Equatorial Undercurrent The seasonal signal of the Undercurrent is not clear, in figures 9 through 12. For the section 145W to 155W, it consists of a general weakness in February and March, and a sharp weakness in August (see Fig. 6). The Undercurrent has a double peak in May to July, and is strong in the last quarter of the year with a peak in late November. Please keep in mind, that velocities should be interpreted as anomalies, thus westward flow is a negative velocity anomaly.

South Equatorial Current In March (see Fig. 9), the core of the SEC at 140°W is at 5°S. To the west, the SEC becomes narrower and shifts northward to reach the Equator by 140°E. The highest velocities are from 180 to 165°E. From 140°W to 155°W, the SEC is being fed from the south and losing water to the south and NEC west of the dateline. The SEC is also feeding the New Guinea Current. In June (see Fig. 10), the SEC is weaker, narrower and, west of 150°W, shifted southward. From 140°W to 150°W, the current's core is still around 5°S, but shifts southward starting at 150°W to 8°S at 155°W. To the west, it shifts northward to 5 to 6°S by 175°E. The highest velocities are found from 175°E to 170°W. West of 155°E, the SEC is less than 3 cm/sec. In

northward to 5 to 6°S by 175°E. The highest velocities are found from 175°E to 170°W. West of 155°E, the SEC is less than 3 cm/sec. In

September (see Fig. 11), the SEC is narrower and stronger from the dateline east to 140°W. The SEC at 140°W is still at 5°S, but shifts northward from 150°W to 165°W to 1 to 2°S, where it has peak velocities between 165°W and 180. West of the dateline, the current weakens, and shifts southward between 170°E to 165°E to 5 to 6°S, where it is fed from the south. The current increases slightly as it feeds the New Guinea Current. In December (see Fig. 12), the SEC is very weak, being greater than 3 cm/sec only east of the dateline. At 140°W, the core lies around 6°S, and the current weakens, narrows, and shifts northward west of 155°W to 4 to 5°S. West of the dateline, the SEC is characterized by meanders, low velocities and eddies.

b. INTERANNUAL VARIABILITY OF THE NEC

Figures 13e and 13f suggest that the North Equatorial Countercurrent crosses the NEC and passes out of the model. Model current vector diagrams show this to be a drawback of the UYT (contour of zonal velocity in latitude and time) diagrams. Actually for the section 145°W-155°W, the Countercurrent disappears in November, 1966. The westward flow south of the Countercurrent is due to either Rossby waves or eddies, as is the eastward flow north of 10° after November 1966. Later in January 1967, the NEC makes a rapid shift southward to 5°N, only to shift northward as the Countercurrent reappears. The beginning of 1962, late 1964 thru early 1965, and 1968 are similar.

In January 1962, the core (velocity maximum) of the NEC is at 14-15°N (see Fig. 13a). After weak easterly flow, the core is at 10°N in March and follows the seasonal signal in position and strength.

14-15°N (see Fig. 13a). After weak easterly flow, the core is at 10°N in March and follows the seasonal signal in position and strength.

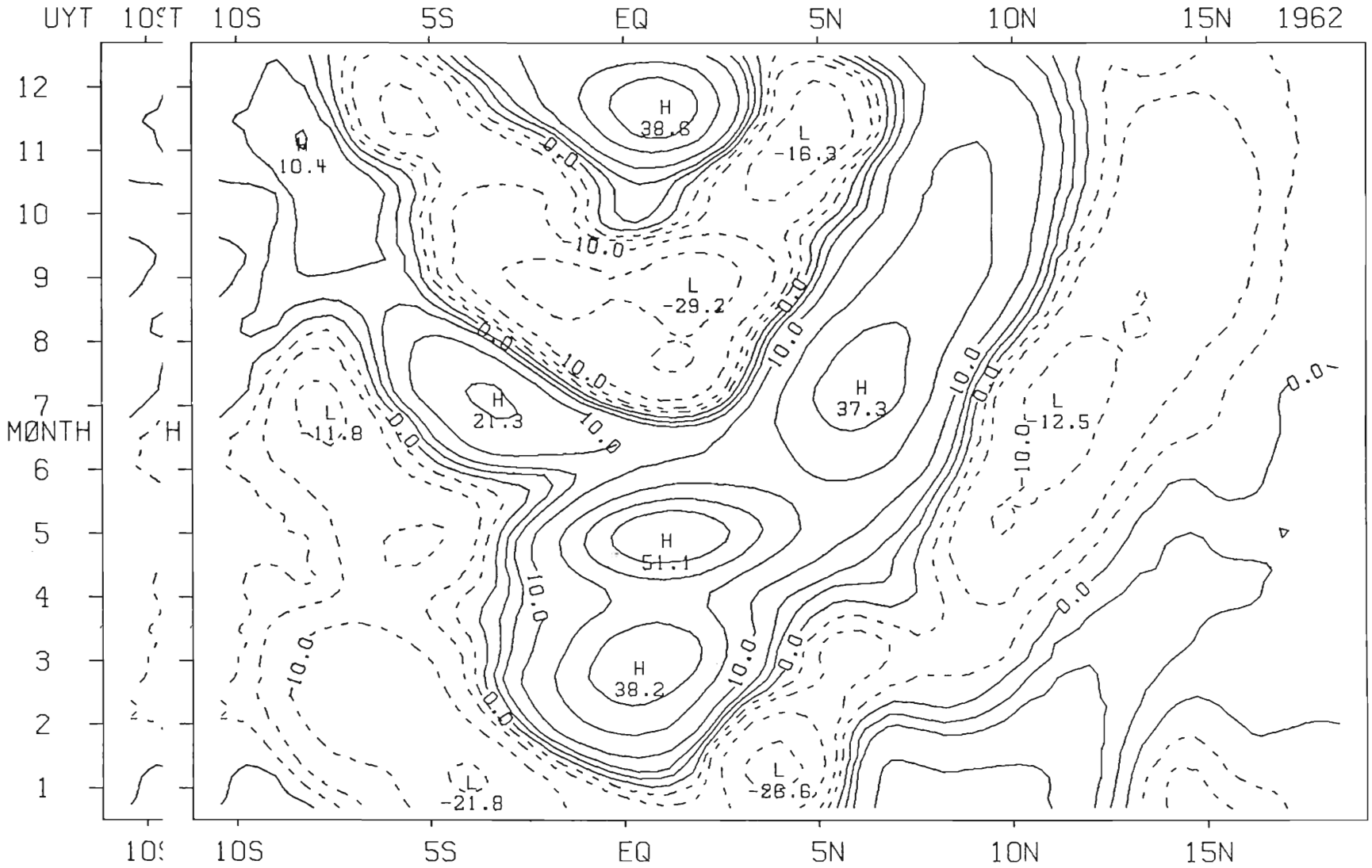
UYT 10ST 10S 5S EQ 5N 10N 15N 1962
MONTH
12
11
10
9
8
7
6
5
4
3
2
1
H 38.8
L -16.3
10.4
L -29.2
H 37.3
L 12.5
H 21.3
L -11.8
H 51.1
H 38.2
L -28.6
L -21.8
0.0
10.0
-10.0
10S 5S EQ 5N 10N 15N

Fig. 13a

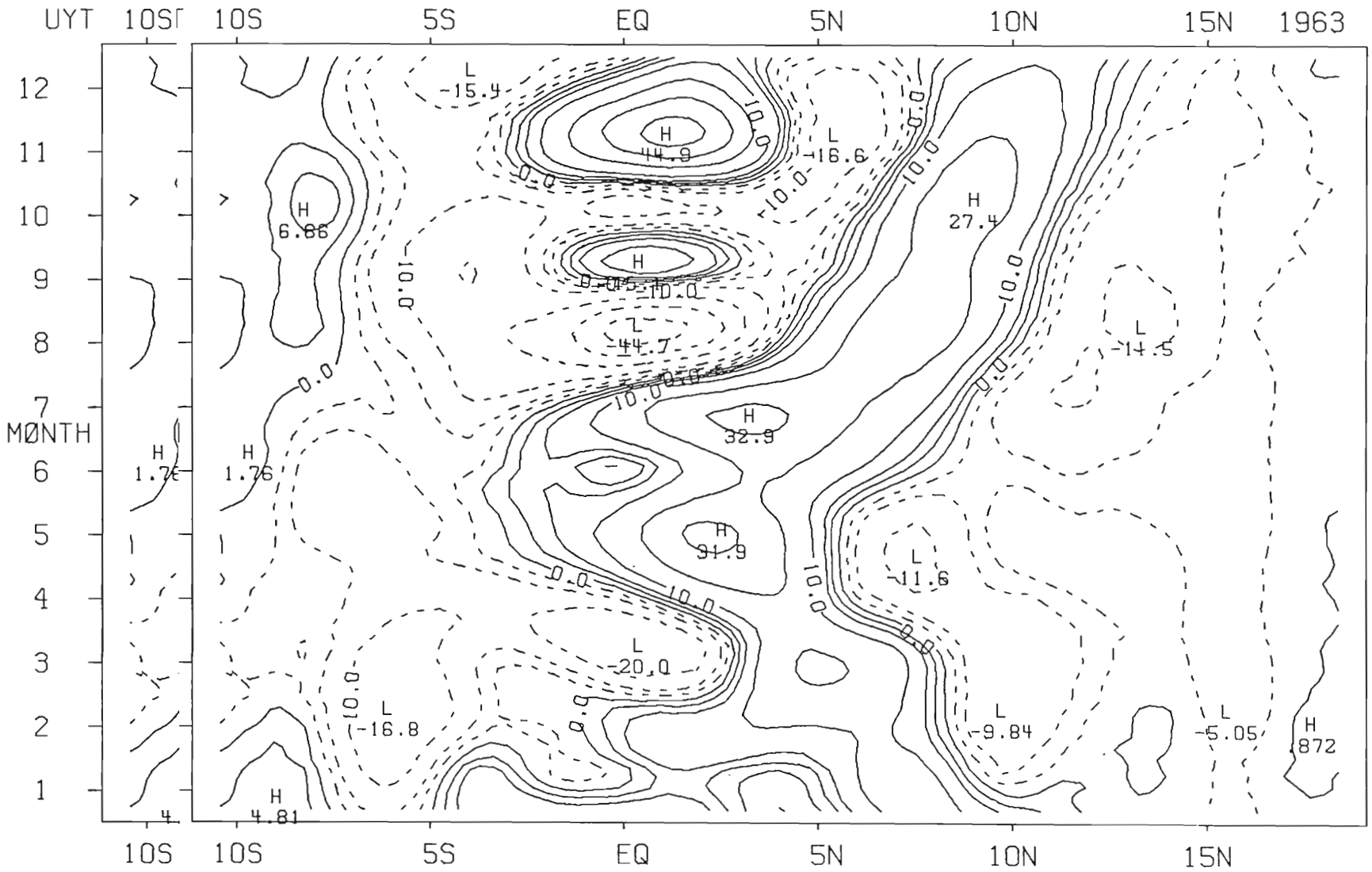
UYT
10S
10S
5S
EQ
5N
10N
15N
1963
MØNTH
12
11
10
9
8
7
6
5
4
3
2
1
L -15.4
H 44.9
L -16.6
H 6.86
H 27.4
H
L -44.7
L -14.5
H 32.9
H 1.76
H 1.76
H 91.9
L -11.6
L -20.0
L -16.8
L -9.84
L -5.05
H 872
H 4.81
10.0
0.0

Fig. 13b

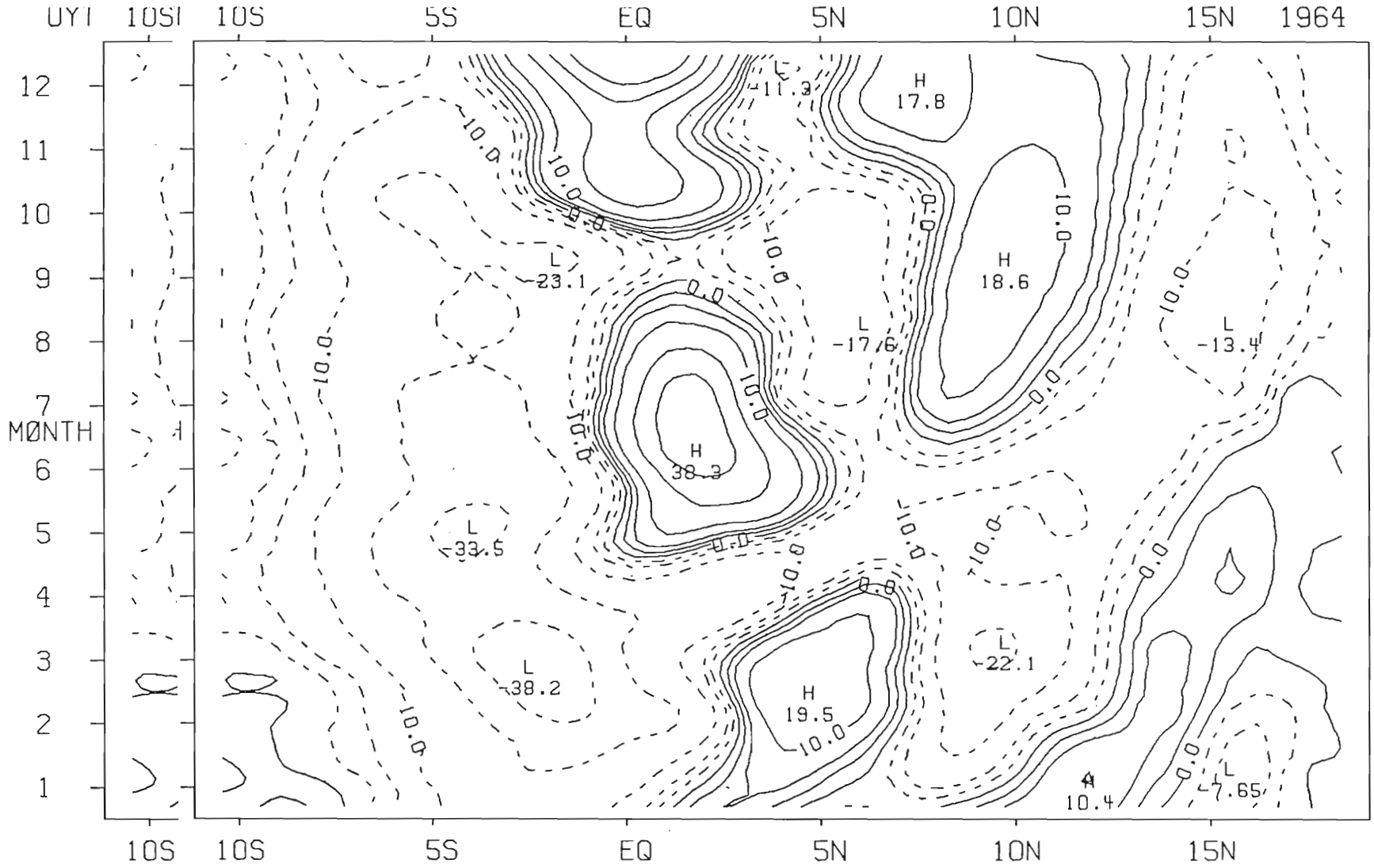
UYI 10SI 10S 5S EQ 5N 10N 15N 1964
12
11
10
9
8
7
MØNTH
6
5
4
3
2
1
10S 10S 5S EQ 5N 10N 15N
L -11.3
H 17.8
L -23.1
H 18.6
L -17.6
L -13.4
H 38.3
L -33.5
L -38.2
H 19.5
L -22.1
L -7.65
10.4
10.0
0.0

Fig. 13c

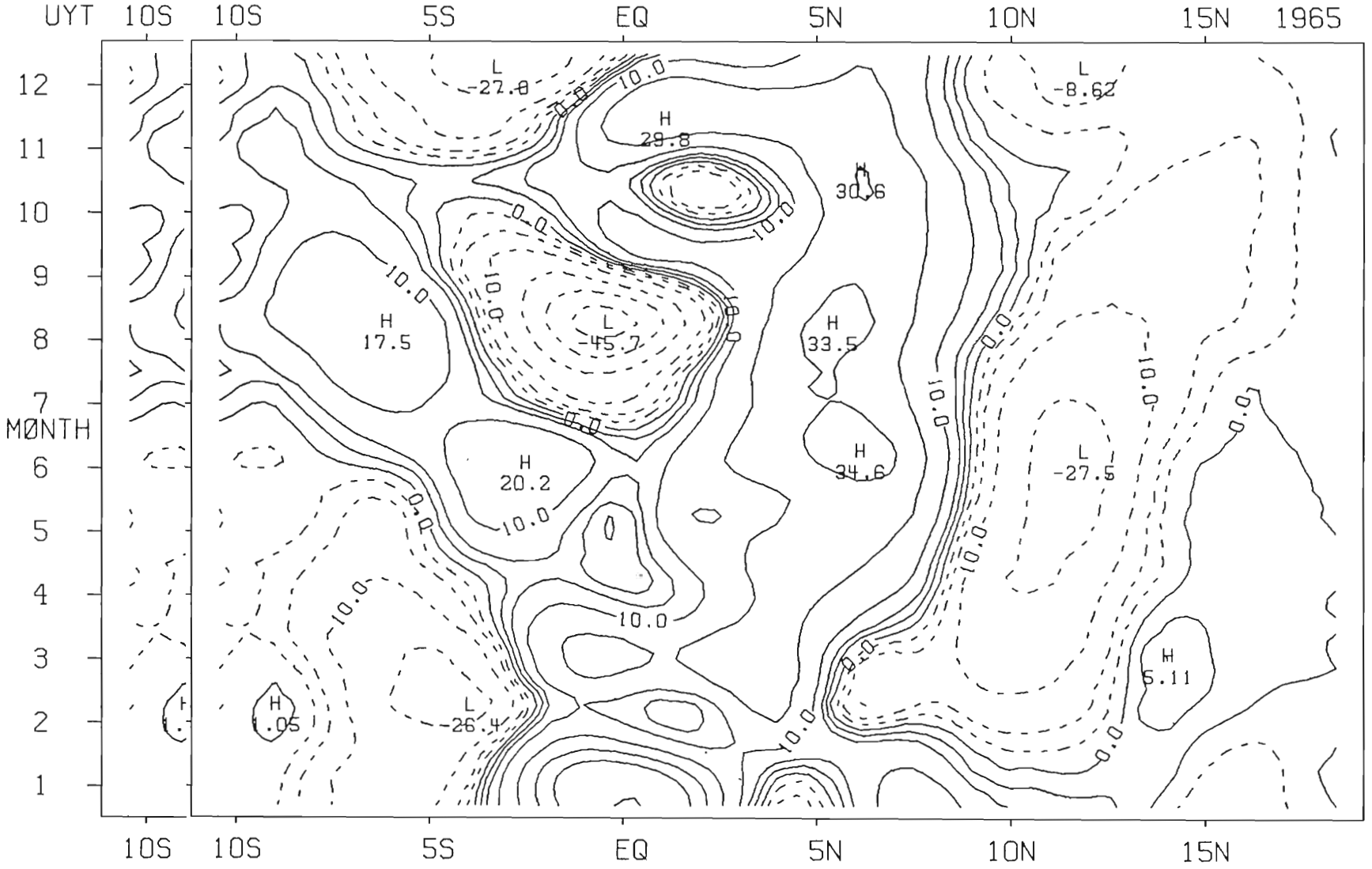
UYT
10S
10S
5S
EQ
5N
10N
15N
1965
MØNTH
12
11
10
9
8
7
6
5
4
3
2
1
L
-27.8
H
29.8
H
30.6
L
-8.62
H
17.5
L
-45.7
H
33.5
H
20.2
H
34.6
L
-27.5
H
5.11
H
.05
L
-26.4
10.0
0.0

Fig. 13d

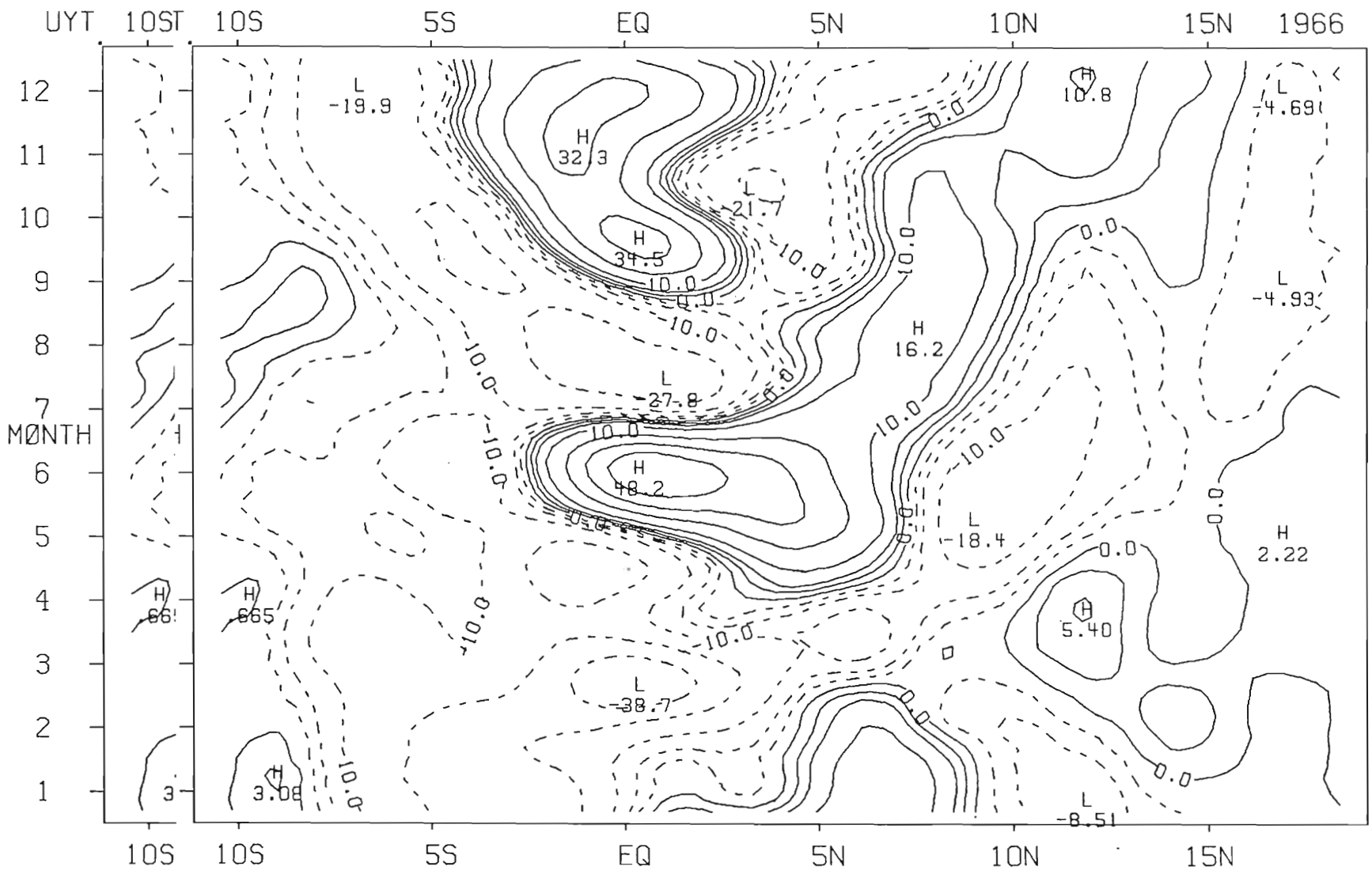
UYT
10ST
10S
5S
EQ
5N
10N
15N
1966
MØNTH
12
11
10
9
8
7
6
5
4
3
2
1
L
-19.9
H
32.3
L
-21.7
H
34.5
10.0
0.0
H
16.2
L
-27.8
H
18.2
L
-18.4
H
10.8
L
-4.69
L
-4.93
H
2.22
H
5.40
L
-38.7
L
-8.51
H
3.08

Fig. 13e

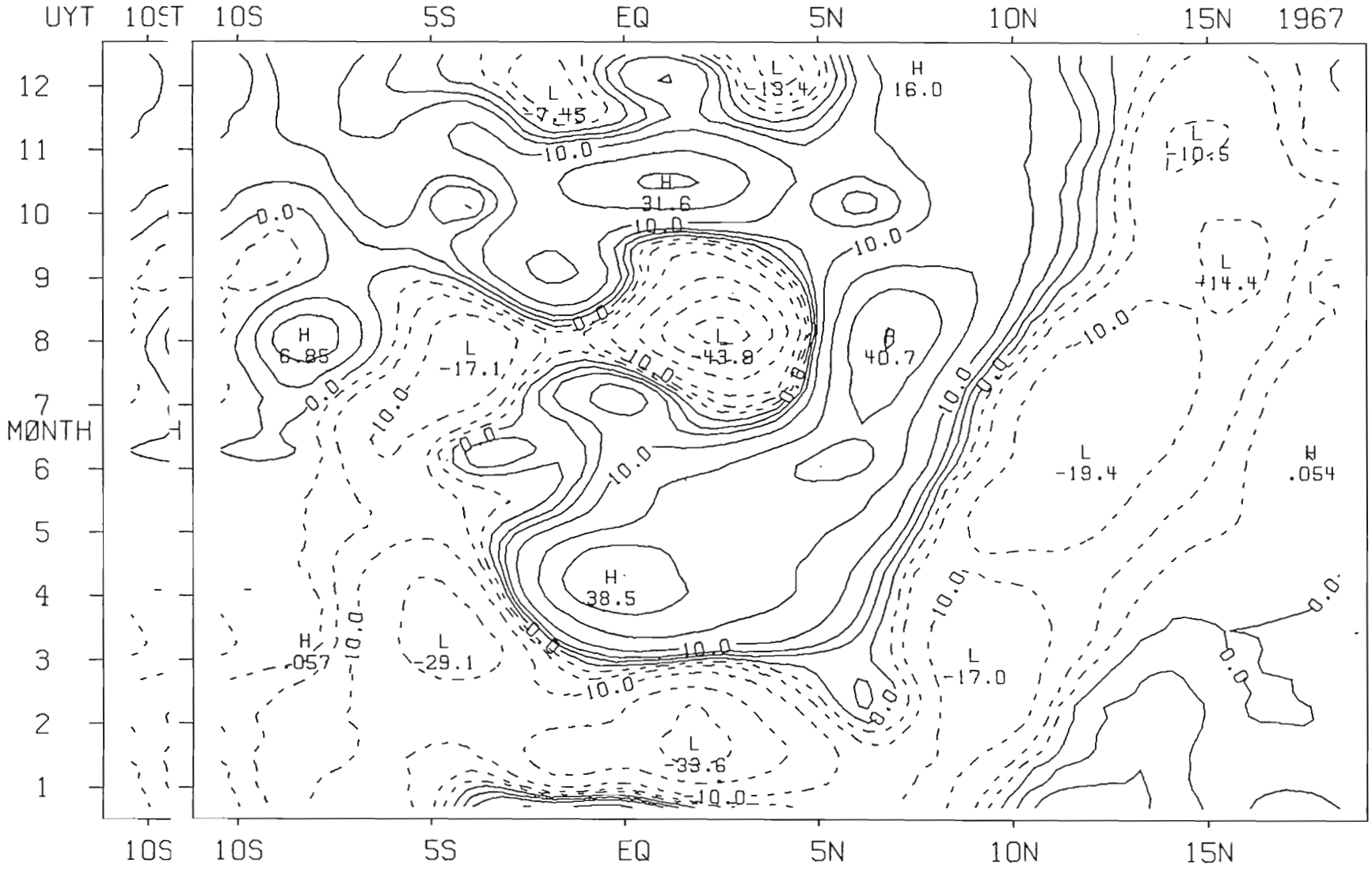
UYT
10ST
10S
5S
EQ
5N
10N
15N
1967
MØNTH
12
11
10
9
8
7
6
5
4
3
2
1
L
-7.45
H
16.0
L
13.4
L
-10.5
H
31.6
10.0
0.0
H
6.85
L
-17.1
L
-43.8
H
40.7
L
+14.4
L
-19.4
H
.054
H
38.5
H
-057
L
-29.1
L
-17.0
L
-33.6

Fig. 13f

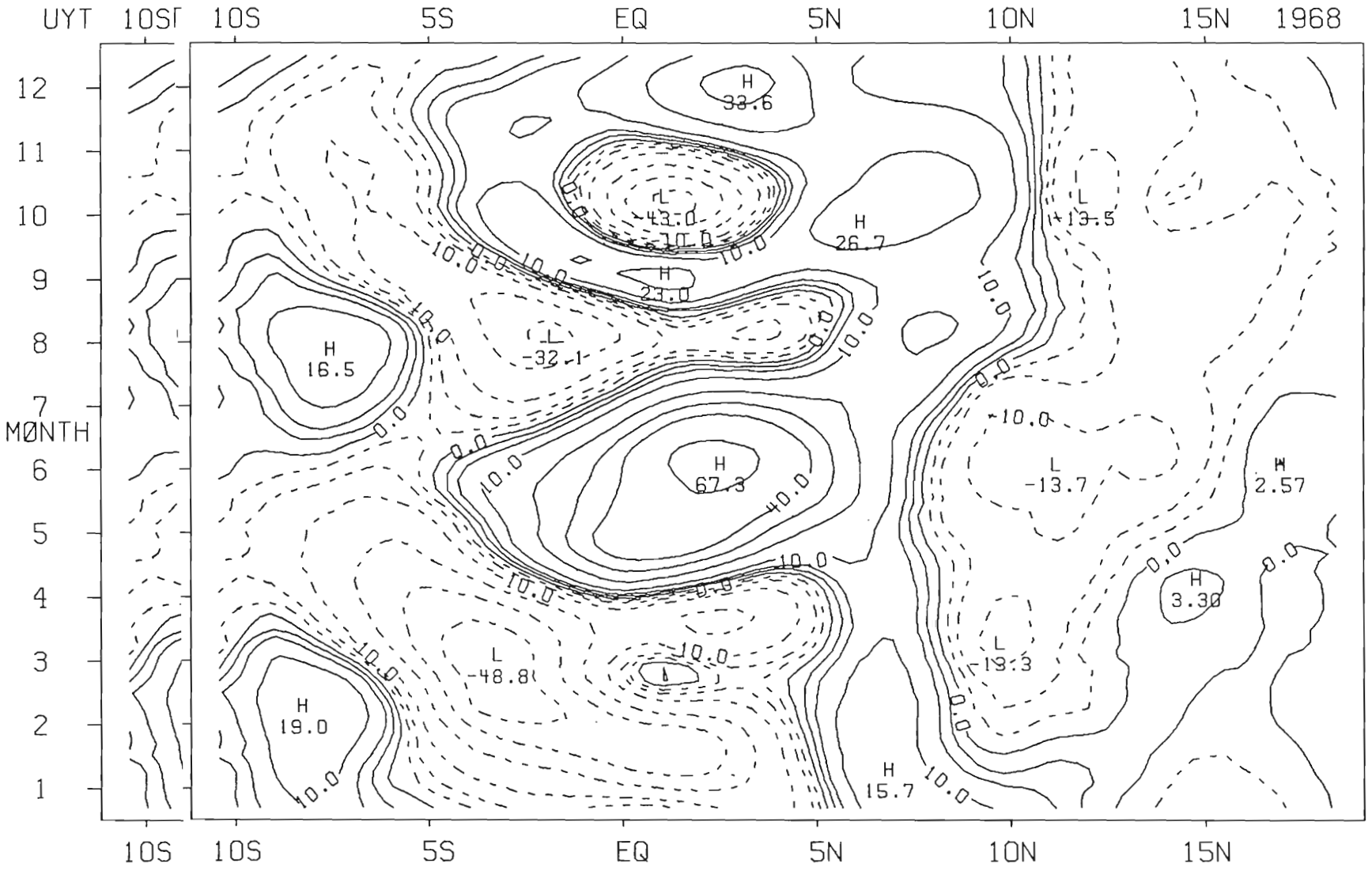
UYT
10S
10S
5S
EQ
5N
10N
15N
1968
MØNTH
12
11
10
9
8
7
6
5
4
3
2
1
H
33.6
L
-43.0
H
26.7
L
-13.5
H
23.0
L
-32.1
H
16.5
H
67.3
L
-13.7
H
2.57
H
3.30
L
-48.8
L
-19.3
H
19.0
H
15.7
10.0
0.0

Fig. 13g

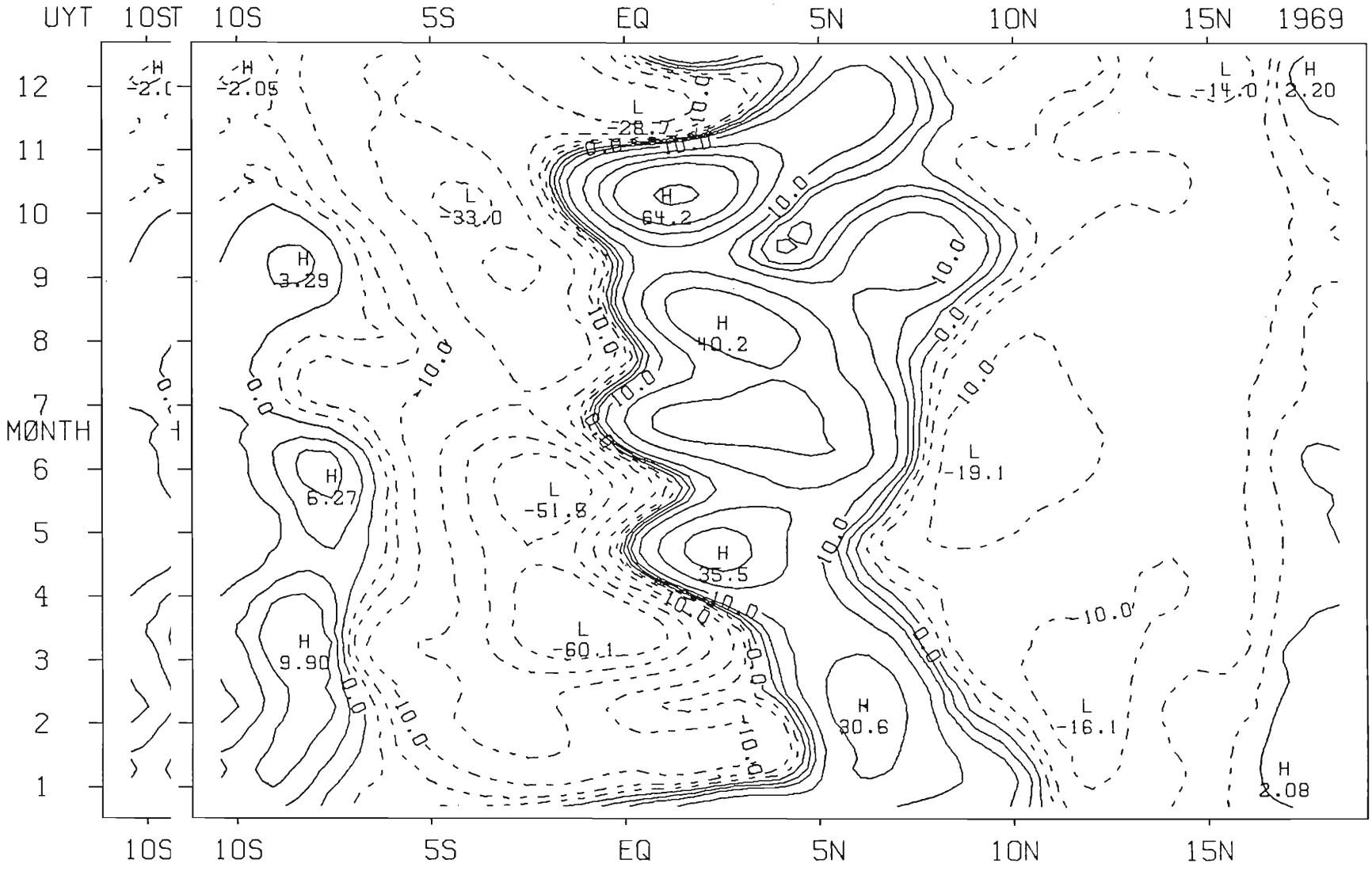
UYT 10ST 10S 5S EQ 5N 10N 15N 1969
MONTH
12
11
10
9
8
7
6
5
4
3
2
1
10S 10S 5S EQ 5N 10N 15N
H 2.20
L -14.0
L -28.7
H 64.2
L -33.0
H 3.29
H 40.2
L -19.1
H 6.27
L -51.8
H 35.5
H 9.90
L -60.1
H 30.6
L -16.1
H 2.08
10.0
0.0
-10.0

Fig. 13h

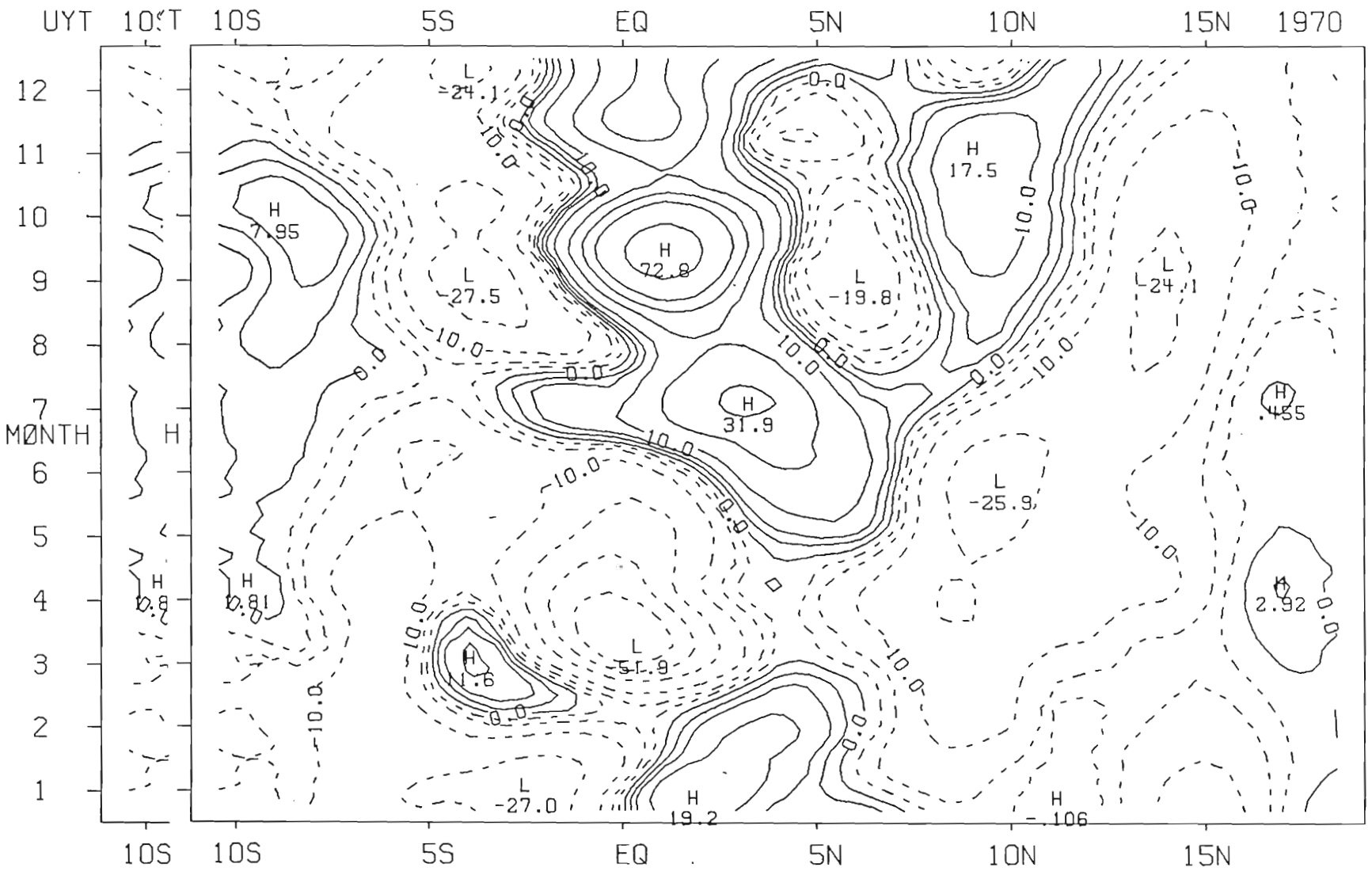
UYT
10S
10S
5S
EQ
5N
10N
15N
1970
MONTH
12
11
10
9
8
7
6
5
4
3
2
1
H
7.95
L
-24.1
L
-27.5
H
72.8
L
-19.8
H
17.5
L
24.1
H
31.9
L
-25.9
H
.455
H
2.92
H
.8
H
.81
H
1.6
L
-51.9
L
-27.0
H
19.2
H
-.106
0.0
10.0
-10.0

Fig. 13i

In January 1963, the NEC's core is located at 15-16°N (see Fig. 13b). By mid-January, a second velocity maximum is forming in the seasonal position of 10°N. Peak velocities occur in both in the latter half of February, though nearly twice as strong in the southern core. The northern core slowly broadens; the southern core makes a rapid southward shift in the first half of April, and strengthens to a stronger peak of 0.12 m s^{-1} at 2.5-3°N in early May. Then the southern core shifts northward; in mid-June, the distinction between cores is lost, and the NEC is broad. In the second half of June, the core is at 11-12°N. The normal seasonal peak is delayed from mid-June to mid-August, and shifted to 13°N.

In late January 1964, the NEC peaks at 15-16°N (see Fig. 13c). The NEC's velocity maximum is found in late April at 10°N, and shifts northward to follow the seasonal tract, with the exception of a peak in late August.

In February 1965, the NEC's core is found at 11°S. For most of 1965, the NEC is strong, broad, and shifted slightly northward (see Fig. 13d). In December, the current shifts rapidly southward, and strengthens to a peak at 11-12°S in late December-early January. For the first two months of 1966, the current continues its southward shift, while weakening (see Fig. 13e). In March, the NEC joins the westward flow that extends from 10°N to 9°S. The NEC separates from this flow in April, and drifts northward to a early seasonal peak at 9°N in late May. In the second half of July, a second velocity maximum develops at 15.5°N, and shifts northward to 17°N by late December. The first shifts
In the second half of July, a second velocity maximum develops at 15.5°N, and shifts northward to 17°N by late December. The first shifts northward to disappear at 11.5-12°N in early October. The events from October 1966 to April 1967 were discussed earlier on page 28.

Located at 7°N in late January 1967, the current shifts northward as per the seasonal signal for the rest of the year, with the exception of two weak peaks in March and late September (see Fig. 13f). In February 1968, the NEC's core is found at 10°N with a weak peak of 0.13 m s^{-1} in March (see Fig. 13g). Thereafter, the seasonal signal is modified by an additional peak in October, and a general southern displacement of the core in the second half of the year. For much of 1968, the NEC is weak and broad.

In 1969, the current is stronger and broader but lacks a well organized core (see Fig. 13h). The seasonal peak in June is displaced 2° south of the seasonal position, and preceeded by a weaker peak in February at 12°N. In late December, the NEC has a weak peak at 15°N, and a second velocity maximum at 9°N, which becomes the core for 1970 (see Fig. 13i). During January and February, the northern maximum decreases as the southern one increases. The core strengthens to a seasonal peak at 9-10°N, and remains strong as it shifts northward. After a slightly weaker peak at 13.5-14°N in late September, the NEC slowly weakens and shifts northward.

In general, the NEC demonstrates a high degree of interannual variability. The NEC has been observed to be characterized by fast westward flow alternating with slow eastward or westward flow (Seckel 1968, 1975). In Fig. 14, this alternating flow can be seen to form bands that are found at higher latitudes with time. A similar structure appears in the model (see Fig. 15). Seckel (1975) sates that this feature is the result of baroclinic eddies.

appears in the model (see Fig. 15). Seckel (1975) sates that this feature is the result of baroclinic eddies.

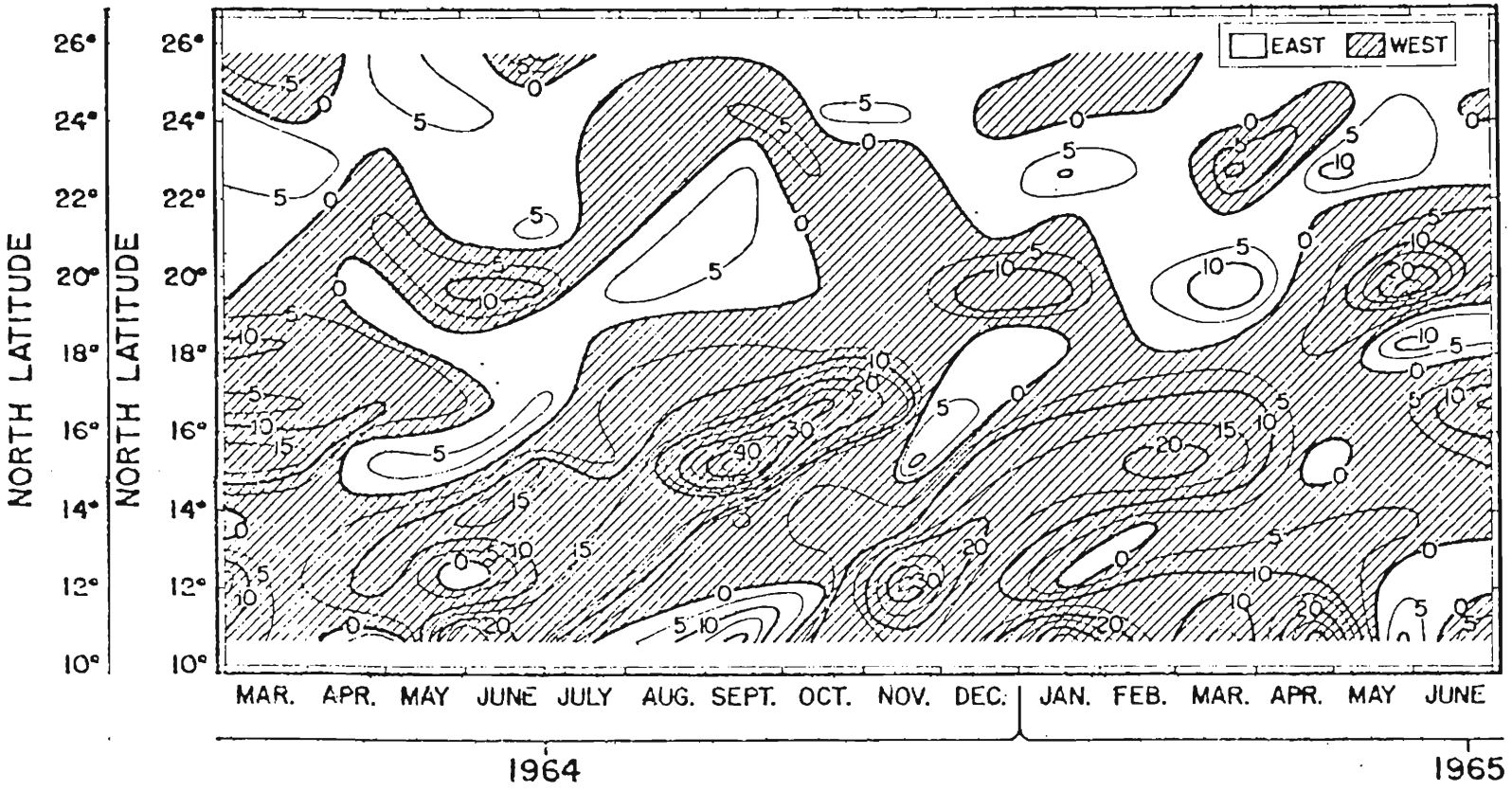

Fi Figure 14. Surface geostrophic zonal flow, relative to 1200 m, contoured in latitude and time. time. Units are 10^{-2} m s^{-1} and hatched area is the westward flowing NEC. Data are from 16 meridiomeridional transects along 148°W by the Trade Wind Oceanographic Investigation. (Fig. 6 of Seckel,Seckel, 1968).

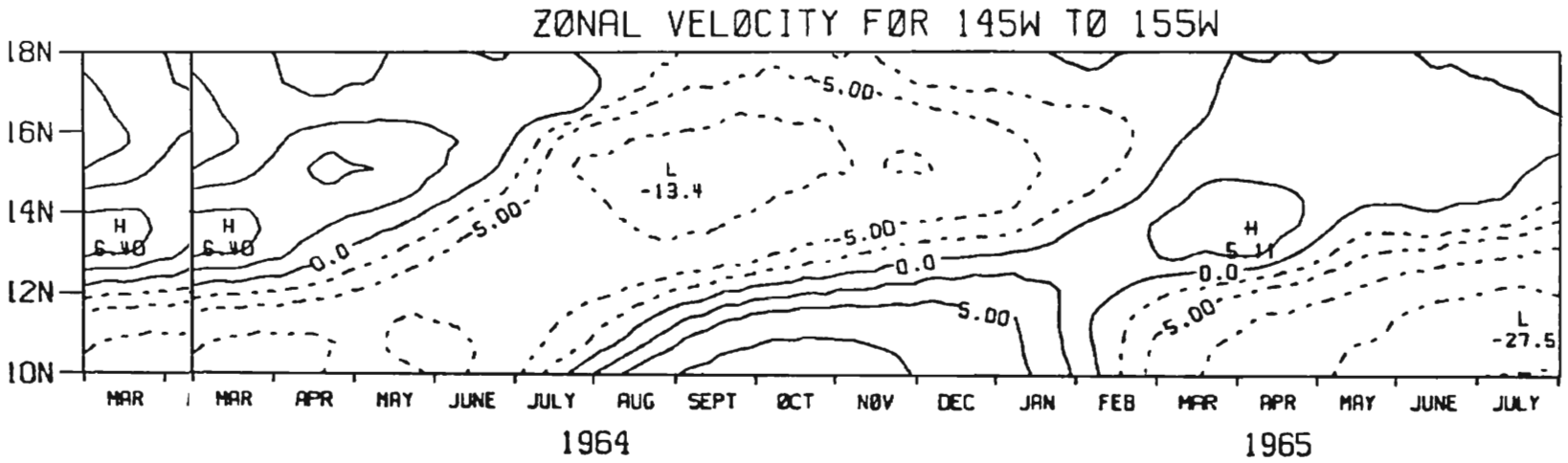

Fig. Figure 15. Contour of model's zonal velocity in latitude and time for the meridional sectionsection zonally averaged from 145°W to 155°W. Units are 10^{-2} m s^{-1} and velocity is determined umined using constant upper layer thickness. Dashed contour lines denote the westward flowingflowing NEC. Note the alternating bands of westward and eastward flow.

C. INTERANNUAL VARIABILITY OF THE NECC

The North Equatorial Countercurrent is a narrow, and often intense (up to 0.41 m s^{-1}) eastward current with high seasonal and interannual variability. It is usually found between the equator and 10°N, and often associated with strong equatorial flows. The NECC is broadest in 1965, thinnest in 1967, and discontinuous in 1962, 1964, 1966, 1967, and 1970.

In June 1962, the NECC is found at 3.7°N separating from the flow at the equator (see Fig. 13a). The seasonal peak is delayed until late July at 6-6.5°N, which is further north than usual, but is the normal location of the current for July. For the remainder of 1962 and the first half of 1963, the current follows the seasonal signal, with the exception of a double seasonal peak. The first peak is at 2.5°N in May; the second at 3-3.5°N in July (see Fig. 13b). At the end of 1963, the current fails to shift southward, but continues to shift northward, and weakens (see Fig. 13c). After February 1964, this current may be an effect of eddies, and not truly part of the NECC.

The NECC is discontinuous in 1964. A second core separates from the equatorial flow in January, peaks at 4-5°N in late February, and disappears at 6.5-7°N in early April. It reforms at 8-8.5°N in the first half of July, and shifts northward to peak at 9.5-10°N in late September. After a rapid southward shift in November, the NECC peaks at 7.5-8°N in December.

In the first quarter of 1965, the NECC shifts southward from 7.5-8°N to a minor velocity peak at 3-3.5°N in mid-March (see Fig. 13d). The current has a seasonal peak of 0.35 m s^{-1} at 6°N in June. The NECC 7.5-8°N to a minor velocity peak at 3-3.5°N in mid-March (see Fig. 13d). The current has a seasonal peak of 0.35 m s^{-1} at 6°N in June. The NECC is strong and broad for the second half of 1965; as expected since 1965 is an El Niño year (Wyrtki 1974b). However, the current is displaced

southward, and lacks the seasonal signal in position. It shifts slightly northward with a few meanders to 6-6.5°N.

In March and much of April 1966, the NECC is absent; it reappears at 4°N in late April (see Fig. 13e). There may be a seasonal peak in June, but the current is overshadowed by the equatorial flow. From which, it separates in July, and shifts northward as per the seasonal signal. At 7.5°N in mid-August, the Countercurrent has an unseasonal peak of 0.16 m s^{-1}, and virtually stops the northward drift. In November, the NECC disappears only to reappear in February 1967; the eastward flow from November to March 1967, north of 10°N, is due to an eddy or Rossby wave (see Fig. 13e, f).

The NECC reforms in the latter part of February 1967, but is soon overwhelmed by eastward flow at the equator. By late May, the NECC takes form and is found at 3.5-4°N, shifting northward and strengthens to a peak of 0.41 m s^{-1} at 6.5-7°N in August. Rapidly weakening, the Countercurrent shifts northward to 9°N by late October. From November 1967 through February 1968, it shifts southward to 6.5°N with a peak of 0.16 m s^{-1} in December or January (see Fig. 13f, g). The NECC is very narrow in March and April, but is connected with a strong eastward equatorial flow from May to mid-July. The peak of the eastward flow is at the right time for the NECC's seasonal peak, though it is displaced too far south. In the last half of July, the NECC separates from the equatorial flow at 6-6.5°N, and shifts northward to 8°N by early September. Thereafter, the Countercurrent shifts southward to 6-6.5°N for a peak of 0.27 m s^{-1} in the first part of October, and a stronger
September. Thereafter, the Countercurrent shifts southward to 6-6.5°N for a peak of 0.27 m s^{-1} in the first part of October, and a stronger peak of 0.34 m s^{-1} at 3°N in December.

In 1969, the NECC is strong, narrow, and heavily influenced by equatorial dynamics (see Fig. 13h). In January, the Countercurrent makes a rapid northward shift to regain its seasonal position. In the second half of February, the NECC has a strong peak of 0.31 m s^{-1} in lieu of the seasonal weakness. From March to mid-November, the Countercurrent is strong but is clearly influenced by equatorial events. In November, the NECC separates from the equatorial flow and shifts northward to reach 6°N by late December.

In 1970, the NECC is weak and narrow when existent (see Fig. 13i). The Countercurrent is south of the seasonal position and dominated by events on the equator during the first quarter of the year. After disappearing in March, it reappears in April, and strengthens to a peak of 0.32 m s^{-1} in July. There is a weak branch of the NECC that shifts northward, with a peak of 0.17 m s^{-1} in mid-November, and appears to split into two in December. The northern split is most likely to be a Rossby wave or eddie. Other than the branch, the NECC is lost in the equatorial flow.

The variability of the model's NECC is similar to the observed variability. Wyrtki (1974b) has the NECC strongest in late 1965, and very strong in late 1963, end of 1968 and beginning of 1969; very weak in early 1964, 1970 (see Fig. 16). The discontinuities or absence of the NECC has been observed by Tsuchiya (1974), who notes that the NECC may either disintegrate or reestablish itself in less than 2 months.

d. INTERANNUAL VARIABILITY OF THE EQUATORIAL UNDERCURRENT

d. INTERANNUAL VARIABILITY OF THE EQUATORIAL UNDERCURRENT

The interpretation of the model data for the Undercurrent is based on the premise that only the variability, not the mean flow, of the

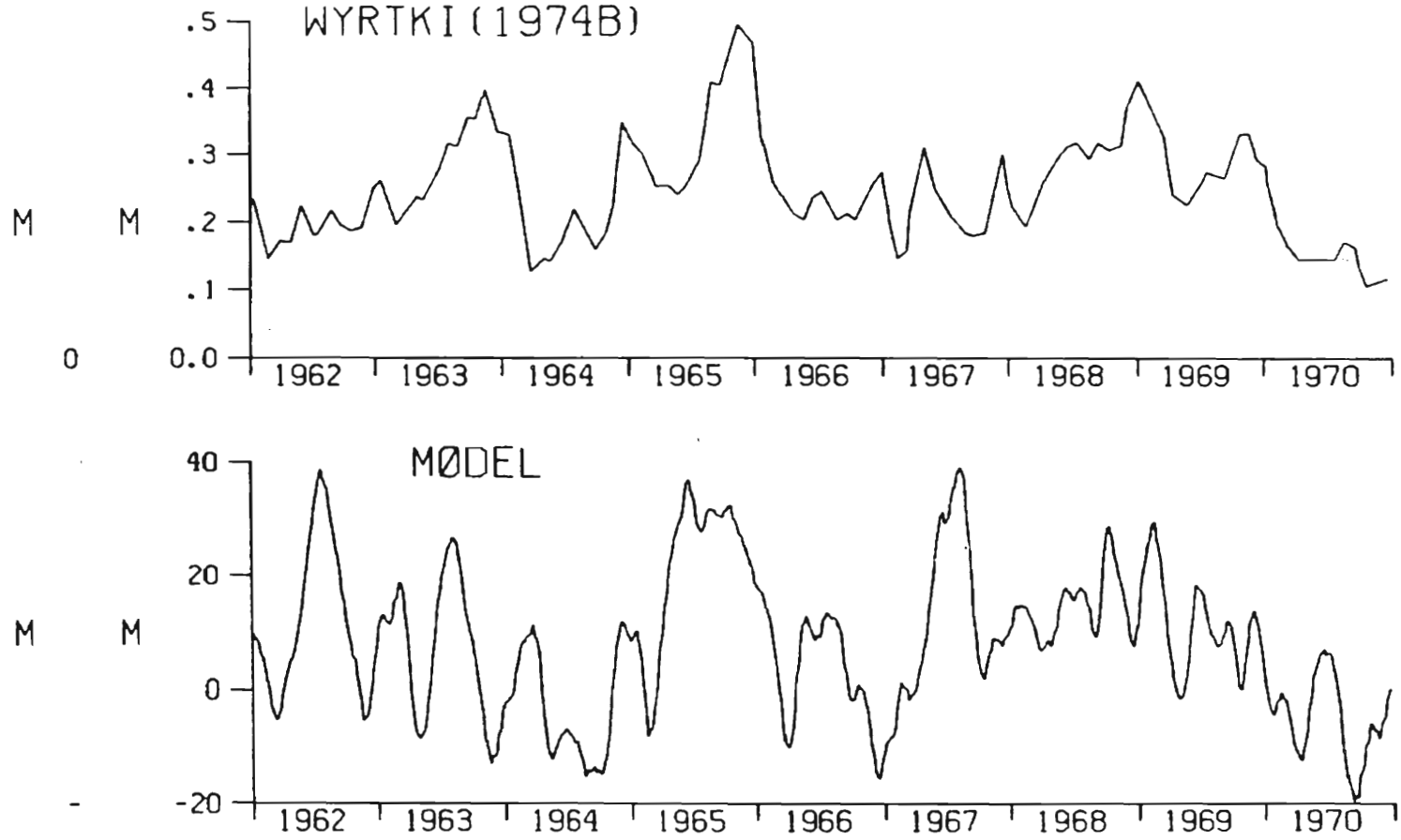

F Figure 16. Sea level difference across the NECC for 140 W to 170 E from Wyrtki (1974b), and th and the difference in upper layer thickness across the model NECC as defined in Table 1 for zonall zonally averaged section 155 W-145 W. Positive difference is for strong current.

Undercurrent is represented in the model. Therefore, for this discussion, all velocities will be taken to be velocity anomalies (Δ).

The variability of the Undercurrent is characterized by being able to change from a high negative velocity anomaly to a high positive anomaly, and back again, in a period of a few months. The Undercurrent is strong in mid-1962, late 1966 thru mid-1967, late 1970, and the strongest from late 1964 until mid-1965. It is weak in late 1963, late 1965 thru early 1966, and the weakest from 1969 thru early 1970.

In the first quarter of 1962, the Undercurrent strengthens to a peak in March, and a stronger peak (Δ = 0.51 m s^{-1}) in May (see Fig. 13a). It is weak in August and September, then strengthens to a seasonal peak (Δ = 0.38 m s^{-1}) in early December. For the first half of 1963, the Undercurrent follows the seasonal signal (see Fig. 13b). After an intense seasonal weakness (Δ = -0.45 m s^{-1}) in August and a minor peak in September, the Undercurrent strengthens from mid-October to a strong peak (Δ = 0.45 m s^{-1}) in November.

In 1964, the seasonal signal is delayed one month with the Undercurrent being weak in January through April (see Fig. 13c). It strengthens from October 1964 to a peak (Δ = 0.52 m s^{-1}) in January 1965 (see Fig. 13c, d). The Undercurrent remains fairly strong through June 1965, but is weak (Δ = -0.46 m s^{-1}) in late August and early September. In October, it strengthens to reach a peak (Δ = 0.3 m s^{-1}) in late November.

The Undercurrent is weak for most of 1966 (see Fig. 13e). It has a very sharp peak (Δ = 0.48 m s^{-1}) in June, a weaker peak in early October, and remains strong until January 1967. The Undercurrent is
a very sharp peak (Δ = 0.48 m s^{-1}) in June, a weaker peak in early October, and remains strong until January 1967. The Undercurrent is weak in early February, but strengthens to a peak of 0.38 m s^{-1} in the

latter half of April (see Fig. 13f). It has a very minor peak in July, the seasonal weakness in August, and a peak of 0.32 m s^{-1} in late October or early November.

The Undercurrent is weak from February to March 1968, and strong for the months of May and June (see Fig. 13g). It has 2 peaks in the latter half of the year; one in September, and the other in December. Between those peaks, the Undercurrent is real weak (Δ = -0.43 m s^{-1}). In late March or early April 1969, it reaches a ten-year low (Δ = -0.6 m s^{-1}), while in late October, it has an extremely strong peak (Δ = 0.64 m s^{-1}) (see Fig. 13h). Even more unusual, is that the Undercurrent weakens and strengthens with a period of 2 months.

In 1970, the Undercurrent is extremely weak (Δ = -0.52 m s^{-1}) in late March, has a minor peak in July, and an extremely strong peak (Δ = 0.73 m s^{-1}) in early October (see Fig. 13i). It remains strong for the rest of the year (see Fig. 17).

For the model's ten degree zonally averaged section centered on 150°W, a comparison of some parameters, of the Undercurrent in the model and observations for the eastern to mid Pacific, show some simalarities. The model's local derivative with time of the zonal velocity is less than 3.7 x 10^{-7} m s^{-2} for the period, 1962 through 1970; while Knauss (1966) estimates it to be on the order of, or less than 10^{-7} m s^{-2}. A comparison of EASTROPAC (April 1968), the DOLPHIN (April-May 1958), and the PIQUERO (July-August 1969) expeditions gives a range of 1.1 to 1.2 m s^{-1} for the variations of zonal velocity; while the model gives a range of 1.4 m s^{-1} (Taft and Jones, 1973).
a range of 1.1 to 1.2 m s^{-1} for the variations of zonal velocity; while the model gives a range of 1.4 m s^{-1} (Taft and Jones, 1973).

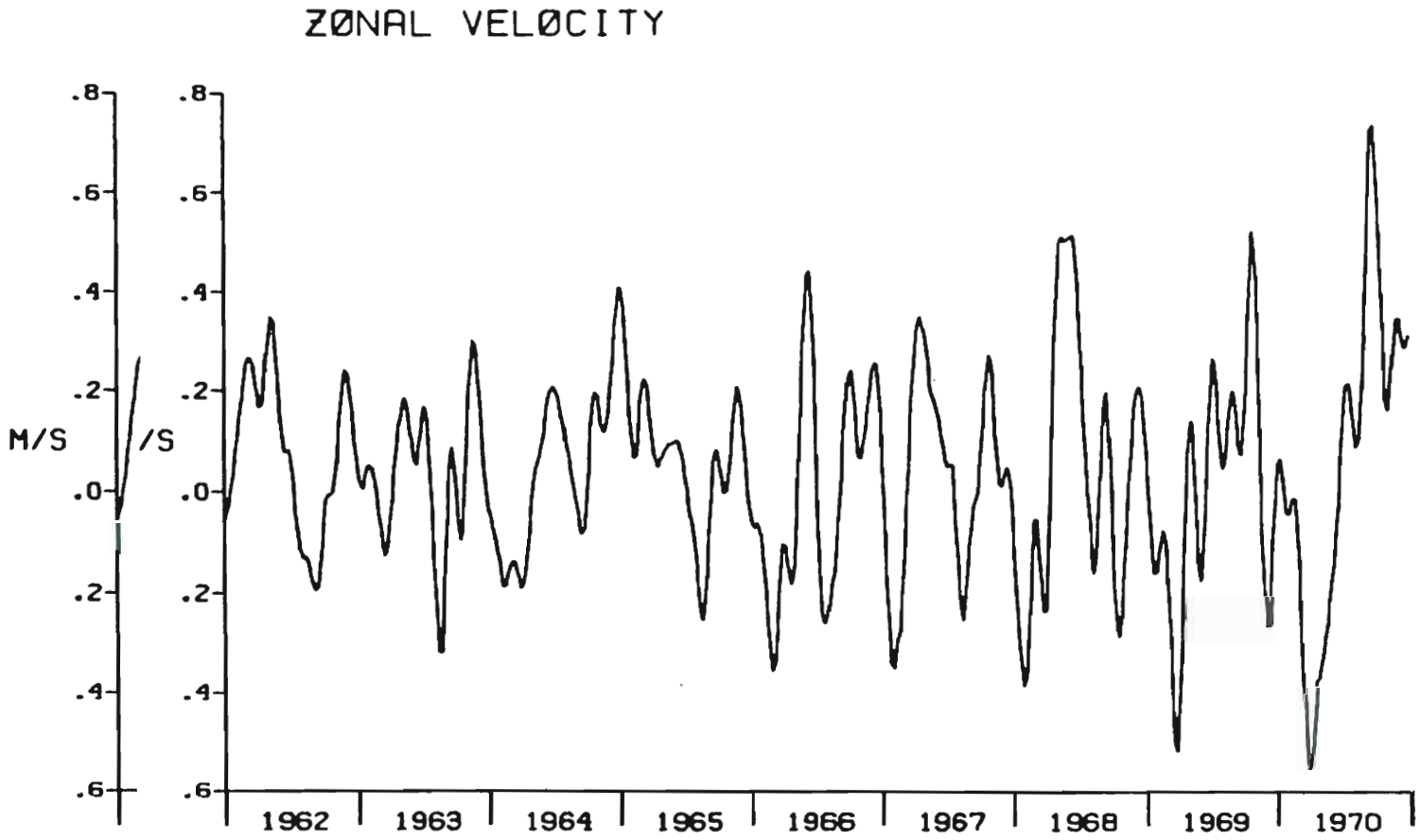

Figure 17. Zonal velocity for the model Equatorial Undercurrent as defined in Table 1 for the zonally averaged section 155 W-145 W. Velocity is determined by using actual upper layer thickness. Velocity at figure's top is eastward.

e. INTERANNUAL VARIABILITY OF THE SEC

For the section, 145°W to 155°W, the SEC's interannual variability dominates the seasonal signal, with the core varying from near the equator to 7°S. In 1964 and 1969, the current is strong and broad with a northward displaced core; while in 1968, the SEC is narrow and meandering. The SEC is interrupted briefly in 1962, 1965, and 1967.

In the first half of 1962, the SEC has the seasonal peak in velocity but its position meanders from 4-5°S in January, to 6-7°S by late February, to 5°S by early May, and to 7-8°S in the first half of July with an unseasonal peak of 0.12 m s^{-1} (see Fig. 13a). In late August, the SEC is interrupted and reforms at 4-5°S. The SEC follows the seasonal signal except it is 1 to 2° south of the normal position where it remains for most of 1963 (see Fig. 13b). In mid-December, 1963, the SEC shifts rapidly northward to 3-4°S.

In 1964, the SEC is stronger and broader than usual (see Fig. 13c). The current is not bounded to the south and does not appreciably decrease or become narrow in July. Until it regains its normal position in mid-October, it is 1 to 2 degrees north of position. In December, it is found 1 to 2 degrees south of position at 6 to 7°S. The SEC shifts northward to regain position by late February 1965 (see Fig. 13d). In the second half of June, the SEC disappears to reform around 2 to 3°S in the latter half of July. The current is disrupted a second time briefly in late October or early November at 4°S and reforms in the same position. It shifts rapidly northward in December to 3°S and a peak velocity of 0.27 m s^{-1}. The SEC is broad at this reforms in the same position. It shifts rapidly northward in December to 3°S and a peak velocity of 0.27 m s^{-1}. The SEC is broad at this point and remains so for the first half of 1966 (see Fig. 13e). The core is not clearly defined from February to June 1966.

In the latter half of August, 1966, the core has a velocity of 0.175 m s^{-1} at 3°S. From August to mid-November, the SEC shifts further south than usual to about 6 to 7°S. In the first quarter of 1967, the SEC shifts north and has a delayed seasonal peak in late March in the normal position (see Fig. 13f). The SEC grows stronger in July to a second weaker peak in August located further south than usual. For September through November 1967, the SEC is absent. The SEC reforms at 2 to 3°S in December, and grows to a very strong peak in mid-March, 1968, at 3 to 4°S (see Fig. 13g). In September and October, the current shifts rapidly south, only to shift northward in November and December to end up around 6°S. The SEC is broader than usual in October and November.

In 1969, the SEC is at its strongest, shifted northward of its normal position but going fairly straight (see Fig. 13h). However, the SEC is more narrow, than it was in 1964, as it is now bounded to the south. The normal seasonal peaks are delayed by 2 months, but in July, the SEC, though broader, shows the usual weakness. The SEC ends the year in the normal position of 5°S, but wider with westward velocities from the Equator to the southern boundary. The SEC is weaker and shifted southward to 7°S for much of the first half of 1970 (see Fig. 13i). For the latter part of the year, the SEC remains stronger than usual and centered on 4 to 5°S without the usual shifts in position.

The observational data for the SEC for the '60's is of an entirely different format than the model data. Wyrtki has derived the height differences across the SEC using island sea level records for the area,
different format than the model data. Wyrtki has derived the height differences across the SEC using island sea level records for the area,
172°W to 150°W and extending south to approximately 17.5°S. Both data

sets are in agreement that the SEC was very strong in 1964, early 1967, 1970, and very weak in late 1965 (see Fig. 18). However, the model has the SEC about average early in 1962 and absent in the latter half of 1967; while height differences have the SEC strong early in 1962, and average in the latter half of 1967. In late 1963, and 1969, the model has the SEC bounded by easterly flow to the South; height differences have the SEC weaker than suggested by the model.

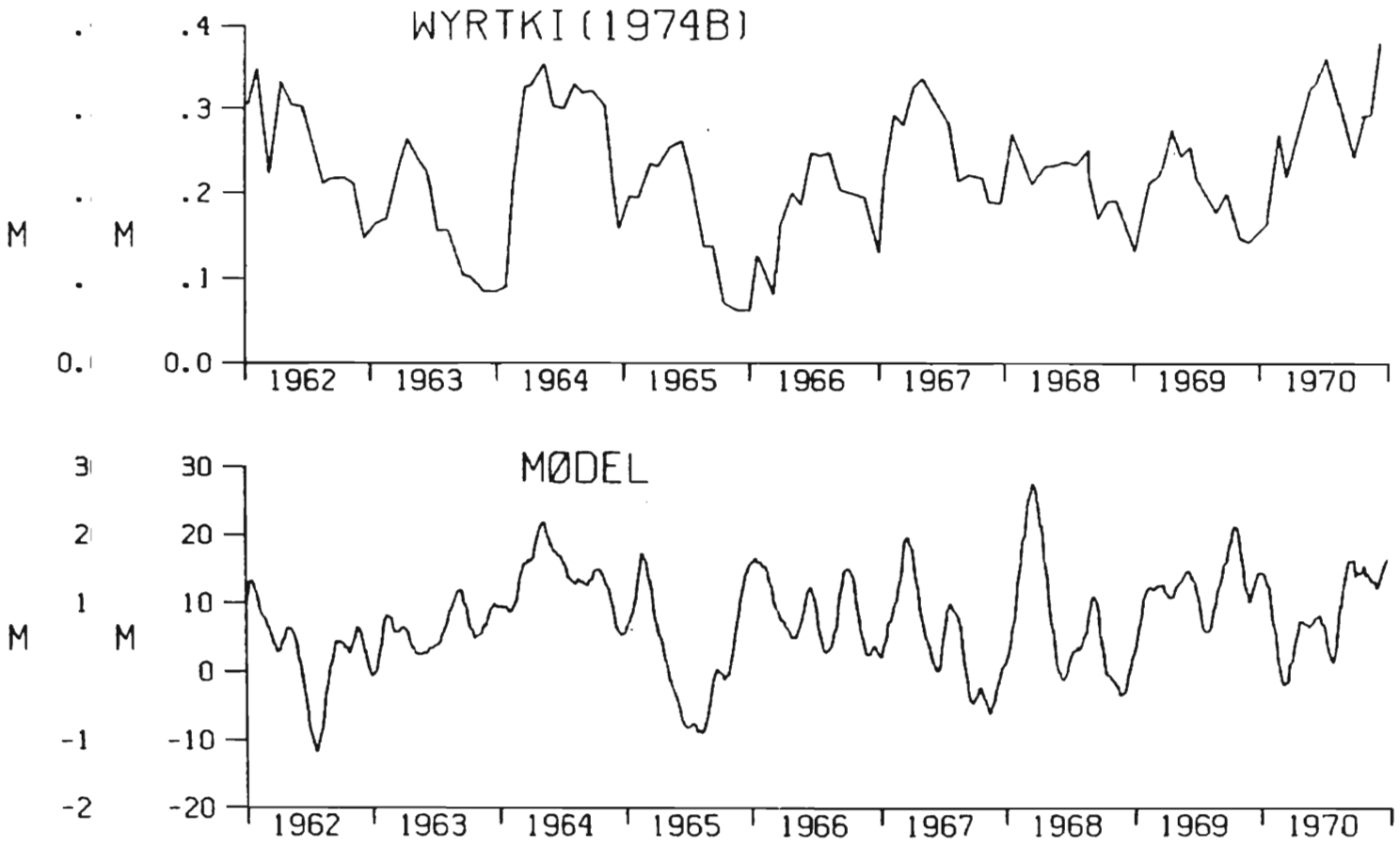

Figure 18. Same as Fig. 16, except for SEC.

4. SUMMARY AND SUGGESTIONS FOR FUTURE WORK

The model and observations give similar descriptions of the variability of the equatorial currents (see Fig. 14, 15, 16, 18, 19). The model has the same general hydrographic features, such as the ridge and trough system, and the east-west tilt of the thermocline (see Fig. 2). These similarities give credence to what is observed in the model.

There is a phase difference in the seasonal signal of the equatorial currents with longitude. This causes the phase relationship between currents to vary from one part of the Pacific to another, and clouds the seasonal picture. The longitudinal dependence of the seasonal signal may be due to modulation of the basic seasonal signal by remote forcing.

A comparison of the two major El Niño years (1965, 1969) yields some major differences. In 1965, the SEC is weak, and the NEC and NECC are strong (Fig. 13d); while in 1969, the SEC and NECC are strong, and the NEC is broad but weak. This suggests that there may be some factor that decides which of the westward flowing currents is to be more strongly affected. However, more than two such events are needed for determination of cause, and confirmation of difference.

The model suggests that the equatorial currents are dominated by interannual variations, and that the classical picture of orderly currents is incorrect. In particular, the NEC is characterized by fast westward flow alternating with slow eastward or westward flow as

currents is incorrect. In particular, the NEC is characterized by fast westward flow alternating with slow eastward or westward flow as

observed by Seckel (1968, 1975) and others. In the model, it appears

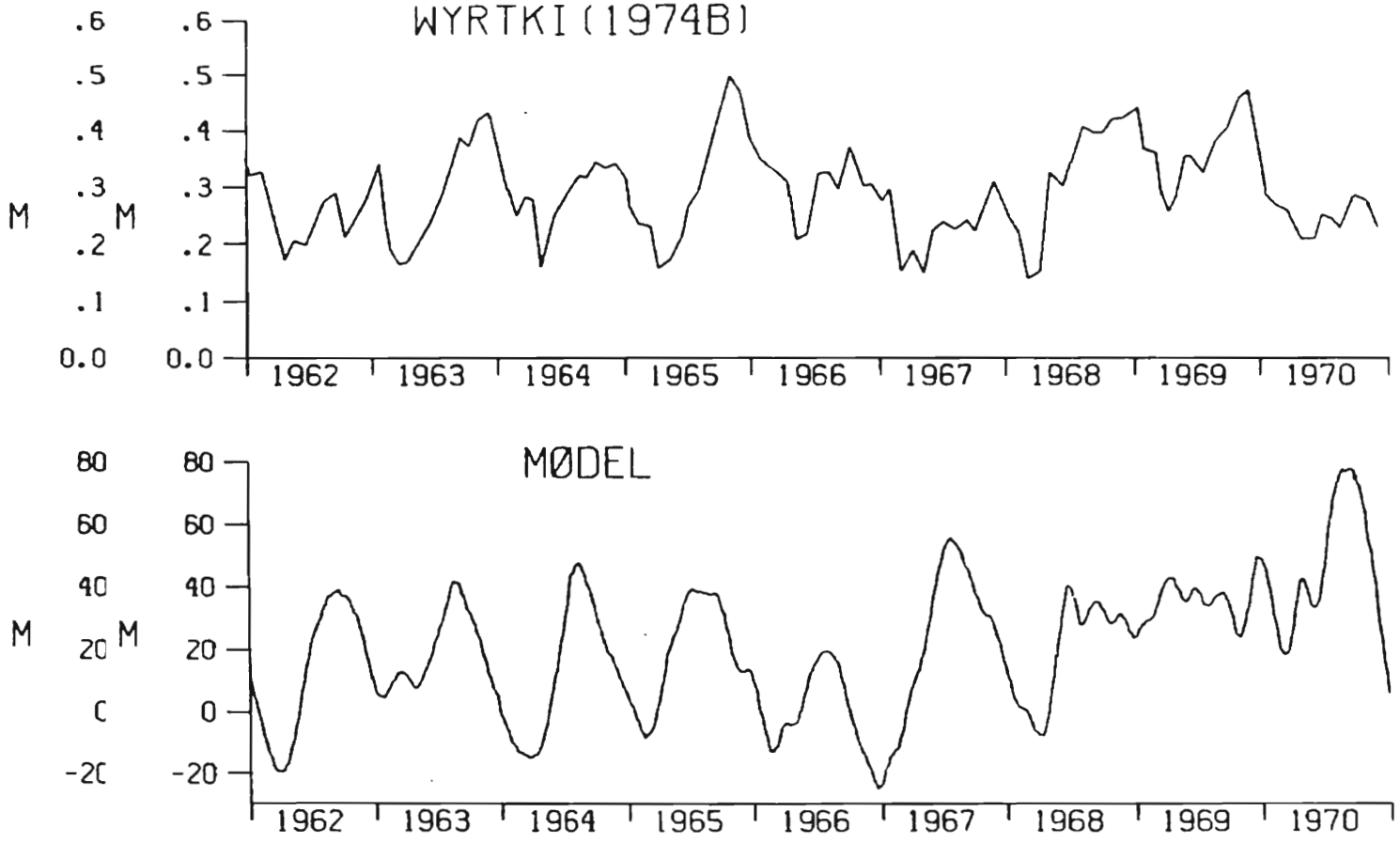

Figure 19. Same as Fig. 18, except for NEC.

that the larger features are caused by either eddies or Rossby waves. The effect must be linear as there are no nonlinearities in the model.

The NECC in the model is a narrow, and often intense current with large changes in position. It's current maximum varies from around 3°N to 10°N. For the region around 150°W, the NECC has a propensity to disappear in the Northern Hemisphere's spring, when it is generally the weakest. As noted by Tsuchiya (1974), the NECC may form or disappear in a time scale of two months or less.

The model's SEC is a fairly continuous current in the region 145°W to 155°W. It's core varies from near the equator to 7°S. The SEC may be broad, or very narrow with extreme shifts in position as in 1968 (see Fig. 13g).

The Equatorial Undercurrent's mean flow is not represented in the model due to the lack of vertical resolution. Observations indicate that it is safe to assume that the Undercurrent does not vary much more than 1° off the equator for the region near 140°W. Therefore, the variability of the equatorial flow in the model may be taken as that of the Undercurrent without being concerned with meandering. No attempt to describe or ascertain Undercurrent meandering has been made. The local derivative with respect to time of the zonal velocity for the zonally average section, 145°-155°W, is of the same magnitude (10^{-7} m s^{-1}) as estimated by Knauss (1966). The range of the zonal velocity is 1.4 m s^{-1} compared to 1.2 m s^{-1} from observations (Taft and Jones, 1973). The differences are slight considering that many of the observations are of short duration and widely spaced in time, and the nature of the model.

These results suggest that it would be worthwhile to investigate the forcing of the interannual variations. Preliminary investigation using the currents, as defined in Table 1 for 145-155°W, found no correlation for Ekman pumping or curl of the wind stress as a major forcing. This needs to be checked out much more carefully as using such a large area may be inappropriate. The effects of an El Niño on equatorial currents can be investigated once the model is run for the 70's. In particular, several studies (e.g., Tsuchiya, 1974) indicate that the NECC is strong (weak) when the ITCZ is in its northern (southern) position, and the ITCZ is displaced southward the year after El Niño (Donguy and Henin, 1980). In the model, the NECC is weak and discontinuous the year after an El Nino or warming (i.e., in 1964, 1966, 1970). However, it is also discontinuous in 1962 and 1967.

The meandering of the Equatorial Undercurrent may be investigated by modulating a mean meridional profile of zonal velocity using the model results. Other projects could include such items as variations in exchange (mixing) rates between currents or oceanic areas.

APPENDIX

A	horizontal eddy viscosity coefficient, 100 $m^2\ s^{-1}$
C	baroclinic phase speed, $(g'H)^{1/2}$, 2.45 $m\ s^{-1}$
g	acceleration due to gravity, 9.8 $m\ s^{-2}$
g'	reduced gravity, $g(\rho_2-\rho_1)/\rho_2$, 0.02 $m\ s^{-2}$
h	upper layer thickness
H	initial upper layer thickness, 300 m
$\hat{i}, \hat{j}, \hat{k}$	x, y, z-directed unit vectors
t	time
u, v	zonal and meridional components of velocity
U, V	zonal and meridional components of transport
$\vec{V}$	total transport vector
x, y, z	tangent plane Cartesian coordinates: x positive eastward, y positive northward and z positive upward.
β	meridional derivative of Coriolis parameter, 2.25 x 10^{-11} $m^{-1}\ s^{-1}$
∇	horizontal gradient operator
∇^2	horizontal Laplacian operator
ρ, ρ_1, ρ_2	densities of seawater
τ_x, τ_y	zonal and meridional components of wind stress, respectively

REFERENCES

Busalacchi, A. J., and J. J. O'Brien, 1980: The seasonal variability in a model of the tropical Pacific. J. Phys. Oceanogr., 10, 1929-1951.

_____ and _____, 1981: Interannual variability of the equatorial Pacific in the 1960's. J. Geophys. Res., (in press).

Donguy, J. R., and C. Henin, 1980: Climatic teleconnections in the western South Pacific with the El Niño phenomenon. J. Phys. Oceanogr., 10, 1952-1958.

Goldenberg, S. B., and J. J. O'Brien, 1981: Time and space variability of tropical Pacific wind stress. Mon. Wea. Rev., 109, 1190-1207.

Knauss, J. A., 1960: Measurements of the Cromwell Current. Deep-Sea Res., 6, 265-286.

_____, 1966: Further measurements and observations on the Cromwell Current. J. Mar. Res., 24, 205-240.

Love, C. M. (editor), 1972: EASTROPAC atlas, Vol. 1 U. S. Dep. Commer., Natl. Mar. Fish. Serv., Circ. 330.

Magnier, Y., H. Rotschi, P. Rual and C. Colin, 1973: Equatorial circulation in the western Pacific. Progress in Oceanography, Vol. 6, Pergamon Press, 29-46.

Masuzawa, J., and K. Nagasaka, 1975: 137°E oceanographic section. J. Mar. Res., 33(suppl.), 109-116.

Seckel, G. R., 1968: A time-sequence oceanographic investigation in the North Pacific tradewind zone. Trans. Amer. Geophys. Union, 49, 377-387.

_____, 1975: Seasonal variability and parameterization of the Pacific North Equatorial Current. Deep-Sea Res. and Oceanogr. Abs., 22, 379-401.

Taft, B. A., and J. H. Jones, 1973: Measurements of the equatorial undercurrent in the eastern Pacific. Progress in Oceanography, Vol. 6, Pergamon Press, 47-110.

Tsuchiya, M., 1974: Variation of the surface geostrophic flow in the undercurrent in the eastern Pacific. Progress in Oceanography, Vol. 6, Pergamon Press, 47-110.

Tsuchiya, M., 1974: Variation of the surface geostrophic flow in the eastern intertropical Pacific Ocean. Fish. Bull., 72, 1075-1086.

Wyrtki, K., 1974a: Sea level and the seasonal fluctuations of the equatorial currents in the western Pacific Ocean. J. Phys. Oceanogr., 4, 91-103.

_____, 1974b: Equatorial currents in the Pacific 1950 to 1970 and their relations to the trade winds. J. Phys. Oceanogr., 4, 372-380.

_____, and G. Meyers, 1975a: The trade wind field over the Pacific Ocean. Part I. The mean field and the mean annual variation. Rep. HIG-75-1, Hawaii Institute of Geophysics, University of Hawaii, 26 pp.

_____, and _____, 1975b: The trade wind field over the Pacific Ocean. Part II. Bimonthly fields of wind stress: 1950 to 1972. Rep. HIG-72-2, Hawaii Institute of Geophysics, University of Hawaii, 16 pp.

_____, 1979: The response of sea surface topography to the 1976 El Niño. J. Phys. Oceanogr., 9, 1223-1231.

_____, et al., 1981: The Hawaii to Tahiti Shuttle Experiment. Science, 211, 22-28.